Extratropical Transition of Tropical Cyclones over the Western North Pacific. Part I: Evolution of Structural Characteristics during the Transition Process

PATRICK A. HARR AND RUSSELL L. ELSBERRY

Department of Meteorology, Naval Postgraduate School, Monterey, California

(Manuscript received 18 January 1999, in final form 7 December 1999)

ABSTRACT

The development of extratropical cyclone structural characteristics that resulted from the extratropical transition of Typhoon (TY) David (1997) and TY Opal (1997) over the western North Pacific is examined. David moved poleward ahead of a midlatitude trough that was moving eastward as the dominant midlatitude circulation feature over the western North Pacific. During the transition, David coupled with the midlatitude trough, which led to the evolution of an intense cyclone that became the primary circulation over the North Pacific. Although Opal also moved poleward ahead of a midlatitude trough, the principal midlatitude feature over the western North Pacific was a preexisting stationary cyclone over the Kamchatka peninsula. During transition, Opal weakened and became a secondary cyclone to the preexisting primary North Pacific cyclone.

The structural characteristics of the evolving extratropical cyclone with respect to each case are examined in the context of the interaction between a vortex and a baroclinic zone using vector-frontogenesis diagnostics for the Lagrangian rate of change of the magnitude and direction of the horizontal gradient of potential temperature. In this framework, total frontogenesis is divided into components that define the magnitude and rotation of the potential temperature gradient. The initial evolution of extratropical cyclone features for both cases was dominated by warm frontogenesis due to the large amount of warm advection on the east side of the decaying tropical cyclone and the deformation field defined by the poleward movement of the tropical cyclone. However, large differences between the components of rotational frontogenesis for David and Opal are observed that are related to the subsequent reintensification of David and weakening of Opal. The differences are attributed to the different midlatitude circulation characteristics into which each tropical cyclone moved. The pattern of rotational frontogenesis associated with TY David reinforced the dynamical support for the coupling of David with the midlatitude trough, which resulted in the development of an intense extratropical cyclone. During the transition of Opal, maximum rotational frontogenesis occurred over the region where Opal interacted with the preexisting midlatitude cyclone. This weakened the coupling between Opal and the midlatitude trough and prevented the development of a separate extratropical cyclone.

One of the unresolved aspects of forecasting extratropical transition is to define when transition has occurred. Although the final extratropical cyclone characteristics may vary greatly from case to case, increased warm frontogenesis seems to be consistent during the initial change from tropical to extratropical characteristics. Therefore, evolution of a frontogenesis parameter is calculated for each case from before transition, through transition, and after transition. In both cases, the rate of increase in frontogenesis peaks at a time that may be defined as the transition time.

1. Introduction

During the summer and autumn seasons of the Northern and Southern Hemispheres, a recurving tropical cyclone (TC) often evolves into a fast-moving and rapidly developing extratropical cyclone that may contain gale-, storm-, or even tropical cyclone–force winds. These transforming TCs often pose a serious threat to maritime activities over several ocean basins in both hemispheres. In response to optimum-track and least-cost ship routing factors, typical summer and early autumn transoceanic shipping is conducted at higher latitudes to take advantage of more favorable wind and wave height conditions along significantly shorter route distances. Over the North Atlantic region, the extratropical transition of a hurricane can impact northern Europe. Therefore, accurate analyses and forecasts of the intensity and movement of transforming TCs are critical. However, the relatively small scale of the TC and the complex physical processes that occur during the transition from tropical to extratropical characteristics present difficult analysis and forecast problems.

Previous studies of extratropical redevelopment of TCs have emphasized important contributions from such factors as preexisting cyclonic vorticity in association with the TC and latent heat release (Palmen 1958;

Corresponding author address: Patrick A. Harr, Code MR/Hp, Department of Meteorology, Root Hall, 589 Dyer Rd., Monterey, CA 93943-5114.
E-mail: paharr@nps.navy.mil

DiMego and Bosart 1982a,b; Anthes 1990; Sinclair 1993; Browning et al. 1998). Even though extratropical transition (ET) cases that occur during summer and early autumn might be expected to have somewhat reduced baroclinic energetics than associated with wintertime cyclone development, ET can have a dramatic influence on the synoptic midlatitude environment spanning the entire ocean basin. Bosart and Lackmann (1995) demonstrated how a transforming hurricane, David (September 1979), modified an initially weak baroclinic environment to enhance conditions that favor extratropical redevelopment.

The result of extratropical cyclone development is dependent on many aspects of the midlatitude circulation. Browning (1990) defined a standard model of cyclone cloud, precipitation, and airflow patterns. Other studies (Davies et al. 1991; Thorncroft et al. 1993; Evans et al. 1994; Schultz et al. 1998; Sinclair and Revell 2000) defined variabilities associated with the structures of maritime cyclones that depend on many large-scale dynamical factors. In particular, Schultz et al. (1998) found that cyclone development in a diffluent (confluent) background flow results in a mature cyclone structure that is meridionally (zonally) oriented with well-defined cold (warm) frontal structures. Several aspects of ET, such as the relative roles of the various characteristics of the TC versus those of the midlatitude circulation into which the TC is moving, are related to the concepts put forth by Schultz et al. (1998). These are important considerations in forecasting the final result of an ET event. For example, it is important to understand whether the intensity of the TC is related to the intensity of the resultant extratropical cyclone after ET. Klein et al. (2000) examined the dependence of the final extratropical cyclone characteristics on various TC features at the beginning of ET and found that the primary influence on the resulting ET was the character of the midlatitude circulation into which the TC is moving. Thus, it is important to examine the structural evolution of extratropical cyclone characteristics during ET under the influence of different midlatitude flow patterns.

This paper examines the development of extratropical cyclone structural characteristics during the ET of two TCs over the western North Pacific. Typhoon (TY) David (September 1997) moved poleward ahead of a midlatitude trough that was the dominant midlatitude circulation feature over the western North Pacific. During ET, David coupled with the midlatitude trough to develop into an intense extratropical cyclone that became the primary midlatitude circulation over the North Pacific basin. Although TY Opal (June 1997) also moved poleward ahead of a midlatitude trough, the dominant midlatitude circulation over the western North Pacific was a large preexisting cyclone northeast of Opal. During ET, Opal weakened and became a secondary cyclone that traveled around the primary preexisting midlatitude cyclone. The focus here is on how the interaction of the TC and the two types of baroclinic environments influenced the basic physical characteristics associated with the development of extratropical cyclone features.

In this study, the development of frontal characteristics is treated as a manifestation of the complex physical processes that take place during ET, since the development of frontal features (defined as increased horizontal gradients of potential temperature θ) signifies the change from a nearly symmetric TC structure to the typical asymmetric extratropical cyclone structure. Furthermore, the evolution of frontal structures is a primary characteristic of a synoptic model for oceanic cyclone development defined by Shapiro and Keyser (1990). In their model, Shapiro and Keyser (1990) propose that oceanic cyclone development proceeds through four stages that consist of an incipient broad baroclinic phase, frontal fracture, bent-back warm front and frontal T bone, and finally a warm-core frontal seclusion. Subsequent studies of oceanic cyclone development by Neiman and Shapiro (1993), Neiman et al. (1993), and Gronas (1995) have identified many of the physical characteristics proposed by Shapiro and Keyser (1990). However, one important difference from the Shapiro and Keyser (1990) model is that the transition event typically starts with an interaction between the decaying TC and a midlatitude baroclinic zone, which could not be considered as an incipient broad baroclinic phase. Vector-frontogenesis diagnostics (Keyser et al. 1988) are well suited for examination of the change in the magnitude of the horizontal θ gradient (scalar frontogenesis) and the direction of the horizontal θ gradient (rotational frontogenesis). Although both components of frontogenesis are related to patterns of deformation, scalar frontogenesis is related to patterns of divergence, while rotational frontogenesis is related to patterns of relative vorticity.

Because the initial stages of ET involve the interaction between a TC and a baroclinic zone, it is hypothesized that the rotational component contributes significantly to the ET process. It will be demonstrated that although the two cases of ET occurred in different midlatitude circulation types, the patterns of maximum *scalar* frontogenesis occur northeast of each transforming TC due to similar patterns of divergence and deformation that result from the movement of a cyclonic vortex into the baroclinic zone. However, large differences are found between the patterns of *rotational* frontogenesis for each case of ET. The differences are related to unique characteristics of each midlatitude circulation pattern that vary the dynamical support, that is, the locations and intensities of ascending and descending motion around the transforming TC. It will be concluded that the variability in rotational frontogenesis is responsible for the different extratropical cyclone characteristics that result from each ET case.

The data used in this study are defined in section 2. The evolution of structural features associated with the ET of TY David is presented in section 3 while the case of TY Opal is presented in section 4. A final aspect of this study addresses the issue of how to recognize when ET of a TC has occurred. The conclusions in section 5

propose a measure of frontogenesis as an indication of the transition time.

2. Data and methodology

The basic synoptic environment during each transition was defined using Navy Operational Global Atmospheric Prediction System (NOGAPS) analyses on a 1° lat–long grid at all mandatory levels from 1000 to 10 hPa. These analyses were produced by the Fleet Numerical Meteorology and Oceanography Center (Hogan and Rosmond 1993). The analyzed fields from NOGAPS were considered to be of sufficient quality because they included important new data sources such as mid- and upper-tropospheric winds derived from geostationary satellite water vapor imagery (Velden et al. 1997). These improve considerably the quality of analyzed fields over relatively data-void regions. The 1° lat–long grid resolution was adequate since the analysis of ET characteristics was concentrated over synoptic scales such that detailed structural characteristics associated with the TC inner circulation were not required.

Visible and infrared imagery from the Geostationary Meteorological Satellite (*GMS-5*) were used to examine the evolution of cloud features during each ET. Passive microwave imagery from the Special Sensor Microwave/Imager (SSM/I) on polar-orbiting satellites was also used to define rain rates associated with ET events. These data were limited to when a satellite pass was made over the transitioning cyclone. A technique defined by Liu and Curry (1992) was used to define a threshold relationship between the atmospheric brightness temperatures at two frequencies and the rain rate. The lower-frequency (19.35 GHz) brightness temperatures were related to radiation emitted by precipitation particles that caused increased temperature values relative to a radiometric cold (ocean) background. The higher-frequency (85.5 GHz) brightness temperatures were related to radiation that was scattered primarily by ice particles suspended in upper levels of clouds and caused decreased temperatures relative to a radiometrically warm background.

Ideally, ET could be considered as an interaction between a vortex and a baroclinic zone in a manner similar to analyses (Doswell 1984, 1985; Davies-Jones 1985; Keyser et al. 1988) with respect to developing midlatitude frontal boundaries. For the ET of the TCs examined in this study, the development of frontal characteristics was taken as a manifestation of various complex physical processes that acted during the transformation of the TC. Furthermore, the nature of the TC suggests that vorticity influences on the development of the extratropical cyclone structures could be large. Therefore, total frontogenesis was decomposed into components that defined the Lagrangian rate of change of the magnitude and direction of the horizontal θ gradient (Keyser et al. 1988). Because the vertical motion can be large in the decaying TC, the original formulation of Keyser et al. (1988) was modified to include the frontogenetical effects due to gradients of vertical motion acting on the horizontal θ gradient. Schultz and Doswell (1999) have also extended the original formulation of Keyser et al. (1988) in their development of conceptual models of upper-level frontogenesis in two characteristic midlatitude flow configurations.

Petterssen (1956) defined atmospheric frontogenesis as the temporal change following a parcel trajectory of the magnitude of the horizontal θ gradient, which is related to horizontal divergence and resultant deformation by

$$\mathbf{F} = \frac{d}{dt}|\nabla_h\theta| = -\frac{1}{2}|\nabla_h\theta|(E\cos 2\beta - \nabla\cdot\mathbf{V}). \quad (1)$$

In this definition, $\mathbf{V}$ is the horizontal wind, E is the resultant of the deformation defined as $E = (E_{\rm st}^2 + E_{\rm sh}^2)^{1/2}$ with $E_{\rm st}$ ($E_{\rm sh}$) defined as the stretching (shearing) deformation, and β is the angle between the local orientation of the isentropes and the orientation of the axis of dilatation. In this application,

$$\frac{d}{dt} = \frac{\partial}{\partial t} + u\frac{\partial}{\partial x} + v\frac{\partial}{\partial y} + \omega\frac{\partial}{\partial p}$$

and the horizontal gradient operator is defined as

$$\nabla_h = \mathbf{i}\frac{\partial}{\partial x} + \mathbf{j}\frac{\partial}{\partial y}.$$

All operations are performed on pressure surfaces. Following Keyser et al. (1988), the vector frontogenesis, $\mathbf{F}$, is resolved into natural coordinates (n, s) such that

$$\mathbf{F} = F_n\mathbf{n} + F_s\mathbf{s}. \quad (2)$$

The n axis points in the direction opposite to $\nabla_h\theta$ (i.e., toward cold air) and is defined as $\mathbf{n} = -|\nabla\theta|^{-1}\nabla\theta$. The s axis is defined by $\mathbf{s} = \mathbf{n}\times\mathbf{k}$ to be locally tangent to the isentrope and to point in the direction of the thermal wind. The component F_n is referred to as the scalar frontogenesis, which defines the magnitude of the Lagrangian rate of change of the horizontal θ gradient:

$$F_n = -\frac{d}{dt}|\nabla_h\theta|. \quad (3a)$$

The component F_s defines the Lagrangian rate of change of the direction of $\nabla_h\theta$:

$$F_s = \mathbf{n}\cdot\left(\mathbf{k}\times\frac{d}{dt}\nabla_h\theta\right). \quad (3b)$$

Keyser et al. (1988) use the conservation of potential temperature for horizontal adiabatic flow to reexpress F_n and F_s in terms of invariant kinematic quantities. In this study, their formulation is expanded to include vertical motion in the thermodynamic equation. Differentiating the equation for conservation of potential temperature in three-dimensional adiabatic flow respective-

ly by x and y defines the components of $d\nabla_h\theta/dt$ (Schultz and Doswell 1999):

$$\frac{d}{dt}\left(\frac{\partial\theta}{\partial x}\right) = -\frac{\partial u}{\partial x}\frac{\partial\theta}{\partial x} - \frac{\partial v}{\partial x}\frac{\partial\theta}{\partial y} - \frac{\partial\omega}{\partial x}\frac{\partial\theta}{\partial p} \quad (4a)$$

$$\frac{d}{dt}\left(\frac{\partial\theta}{\partial y}\right) = -\frac{\partial u}{\partial y}\frac{\partial\theta}{\partial x} - \frac{\partial v}{\partial y}\frac{\partial\theta}{\partial y} - \frac{\partial\omega}{\partial y}\frac{\partial\theta}{\partial p}. \quad (4b)$$

The vector-frontogenesis components in (3a), (3b) can now be rewritten:

$$F_n = -|\nabla_h\theta|^{-1}\left[\frac{\partial\theta}{\partial x}\frac{d}{dt}\left(\frac{\partial\theta}{\partial x}\right) + \frac{\partial\theta}{\partial y}\frac{d}{dt}\left(\frac{\partial\theta}{\partial y}\right)\right], \quad (5a)$$

$$F_s = -|\nabla_h\theta|^{-1}\left[\frac{\partial\theta}{\partial y}\frac{d}{dt}\left(\frac{\partial\theta}{\partial x}\right) + \frac{\partial\theta}{\partial x}\frac{d}{dt}\left(\frac{\partial\theta}{\partial y}\right)\right]. \quad (5b)$$

Combination of (4a), (4b) and (5a), (5b) provides the following expressions for the vector-frontogenesis components:

$$F_n = -|\nabla_h\theta|^{-1}\left[\frac{\partial\theta}{\partial x}\left(-\frac{\partial u}{\partial x}\frac{\partial\theta}{\partial x} - \frac{\partial v}{\partial x}\frac{\partial\theta}{\partial y}\right) + \frac{\partial\theta}{\partial y}\left(-\frac{\partial u}{\partial y}\frac{\partial\theta}{\partial x} - \frac{\partial v}{\partial y}\frac{\partial\theta}{\partial y}\right) + \frac{\partial\theta}{\partial p}\left(-\frac{\partial\omega}{\partial x}\frac{\partial\theta}{\partial x} - \frac{\partial\omega}{\partial y}\frac{\partial\theta}{\partial y}\right)\right] \quad (6a)$$

F_n-div F_n-def F_n-tilt

$$F_s = -|\nabla_h\theta|^{-1}\left[\frac{\partial\theta}{\partial y}\left(-\frac{\partial u}{\partial x}\frac{\partial\theta}{\partial x} - \frac{\partial v}{\partial x}\frac{\partial\theta}{\partial y}\right) - \frac{\partial\theta}{\partial x}\left(-\frac{\partial u}{\partial y}\frac{\partial\theta}{\partial x} - \frac{\partial v}{\partial y}\frac{\partial\theta}{\partial y}\right) + \frac{\partial\theta}{\partial p}\left(\frac{\partial\omega}{\partial y}\frac{\partial\theta}{\partial x} - \frac{\partial\omega}{\partial x}\frac{\partial\theta}{\partial y}\right)\right]. \quad (6b)$$

F_s-vor F_s-def F_n-tilt

Each term in the equations for the vector-frontogenesis components are labeled to define their contribution to the overall component. The terms labeled F_n-div (F_s-vor) represent the contribution to scalar (rotational) frontogenesis due to divergence (relative vorticity). The contribution to scalar (rotational) frontogenesis from horizontal deformation is labeled F_n-def (F_s-def). The contribution to scalar (rotational) tilting frontogenesis from gradients of vertical velocity acting on the horizontal θ gradient is defined as F_n-tilt (F_s-tilt).

The interpretations of the vector-frontogenesis components are aided by examining the formulations of the F_n and F_s components in their invariant form as defined by Keyser et al. (1998) and modified to include the tilting components as defined by Schultz and Doswell (1999):

$$F_n = \frac{1}{2}|\nabla\theta|(\nabla_h\cdot\mathbf{V} - E\cos 2\beta) - \frac{\partial\theta}{\partial p}(\nabla_h\omega\cdot\nabla_h\theta), \quad (7a)$$

$$F_s = \frac{1}{2}|\nabla\theta|(\mathbf{k}\cdot\nabla_h\times\mathbf{V}_h + E\sin 2\beta) - \frac{\partial\theta}{\partial p}\mathbf{k}\cdot(\nabla_h\omega\times\nabla_h\theta). \quad (7b)$$

The horizontal contributions to F_n are equivalent to (1), which defines deformation to be frontogenetic when the angle between the axis of dilatation and the isentropes is less than 45°, and convergence is frontogenetic regardless of the orientation of the isentropes. The tilting term contributes to scalar frontogenesis when the gradient of vertical velocity is in the same direction as the gradient of θ. From (7b), the tilting contribution to rotational frontogenesis is zero if the vertical velocity and θ gradients are aligned. Tilting rotational frontogenesis is a maximum when the vertical velocity and θ gradients are perpendicular, which also indicates that there is no tilting frontogenesis contribution to F_n. Further inspection of (7b) indicates that deformation contributes to the cyclonic (anticyclonic) rotation of the gradient of θ when the isentropes are oriented between 0° and 90° cyclonic (anticyclonic) to the axis of dilatation. Also, cyclonic (anticyclonic) relative vorticity acts to rotate the gradient of θ in a cyclonic (anticyclonic) direction.

Keyser et al. (1988, 1992) used this association to interpret the scalar or across-isentrope component to forcing over space scales and timescales associated with frontogenesis. The rotational or along-isentrope component was associated with forcing due to the relative flow through the baroclinic wave and was characterized by wave-scale forcing patterns (i.e., forcing over midlatitude synoptic space scales and timescales). In this analysis of ET, the intent is to examine the utility of this type of partitioning of the forcing of frontogenesis, and specifically to examine the relative roles of frontal-scale and wave-scale forcing on each transition as it relates to the evolving cloud patterns.

3. Extratropical transition of TY David (September 1997)

Typhoon David made its closest approach to Japan at 0000 UTC 19 September (Fig. 1a). The sea level pressure (SLP) distribution broadened when David

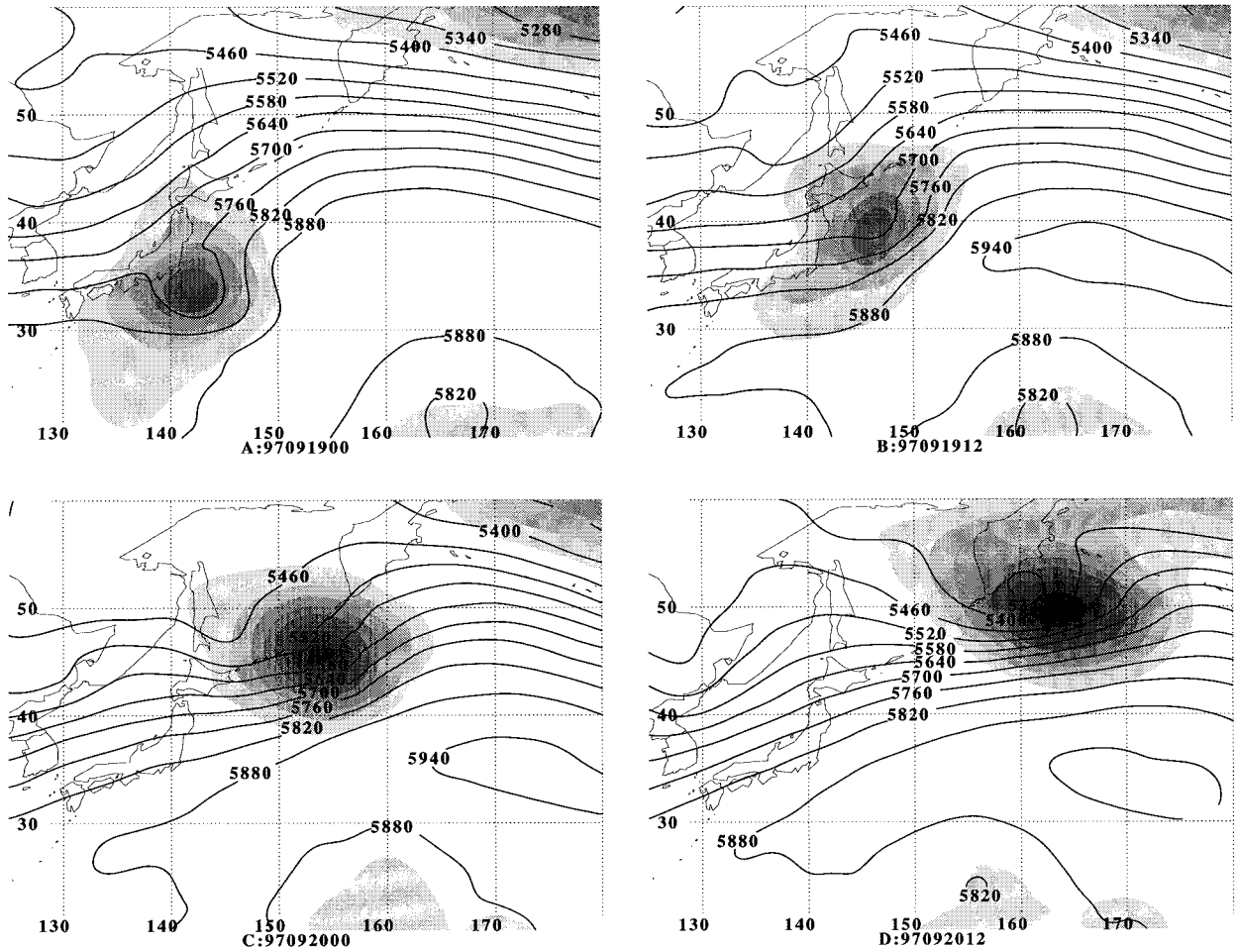

FIG. 1. Analyzed 500-hPa heights (m) and sea level pressure (shaded in 4-hPa increments beginning 1004 hPa) for TY David at the times (year, month, day, hour) indicated beneath each panel.

moved past Japan at 1200 UTC 19 September (Fig. 1b), and the decaying TC was depicted as an open wave in the 500-hPa flow ahead of a larger-scale midlatitude wave that was moving off the Asian mainland north of the Korean peninsula. Infrared (IR) satellite imagery at 1232 UTC 19 September (Fig. 2a) indicated a TC with greatly reduced deep convection south of an extensive cloud pattern that had penetrated northward and then eastward into the midlatitudes. Rain rates derived from SSM/I observations at 0919 UTC 19 September (Fig. 3a) indicated that the extensive cloud pattern consisted mainly of high clouds since significant rain amounts were found only to the immediate north of the TC center. The delta-shaped precipitation region was typical of weakening TCs that move poleward near the islands of Japan (Shimazu 1998).

When David moved northeast of Japan on 0000 UTC 20 September (Fig. 1c), the decaying TC began to reintensify into a significant extratropical cyclone. As David approached the midlatitude wave that was moving off the Asian mainland, a large cloud shield (Fig. 2b) existed to the north of the now reintensifying extratropical cyclone near 46°N, 154°E. Some indication of deep convection existed on the eastern edge of the low-level center, which might have been remnants of the tropical characteristics. However, SSM/I rain rates (Fig. 3b) indicated that significant rainfall was limited to the large cloud shield north of the TC center. Furthermore, the most intense precipitation was organized in two bands located northeast of the low-level center with a west-to-east orientation.

At 1200 UTC 20 September, lower- and upper-level circulations (Fig. 1d) continued to intensify and the SLP reached a minimum of 969 hPa. The IR satellite imagery (Fig. 2c) indicated that the only significant clouds were north of the circulation center. Although an apparent frontal boundary extended southwestward from the center, little organized cloudiness was associated with what might have been a temperature or moisture boundary between cooler air advected around the north and west side of the circulation and warmer air ahead of the circulation. Although no SSM/I data were available at this

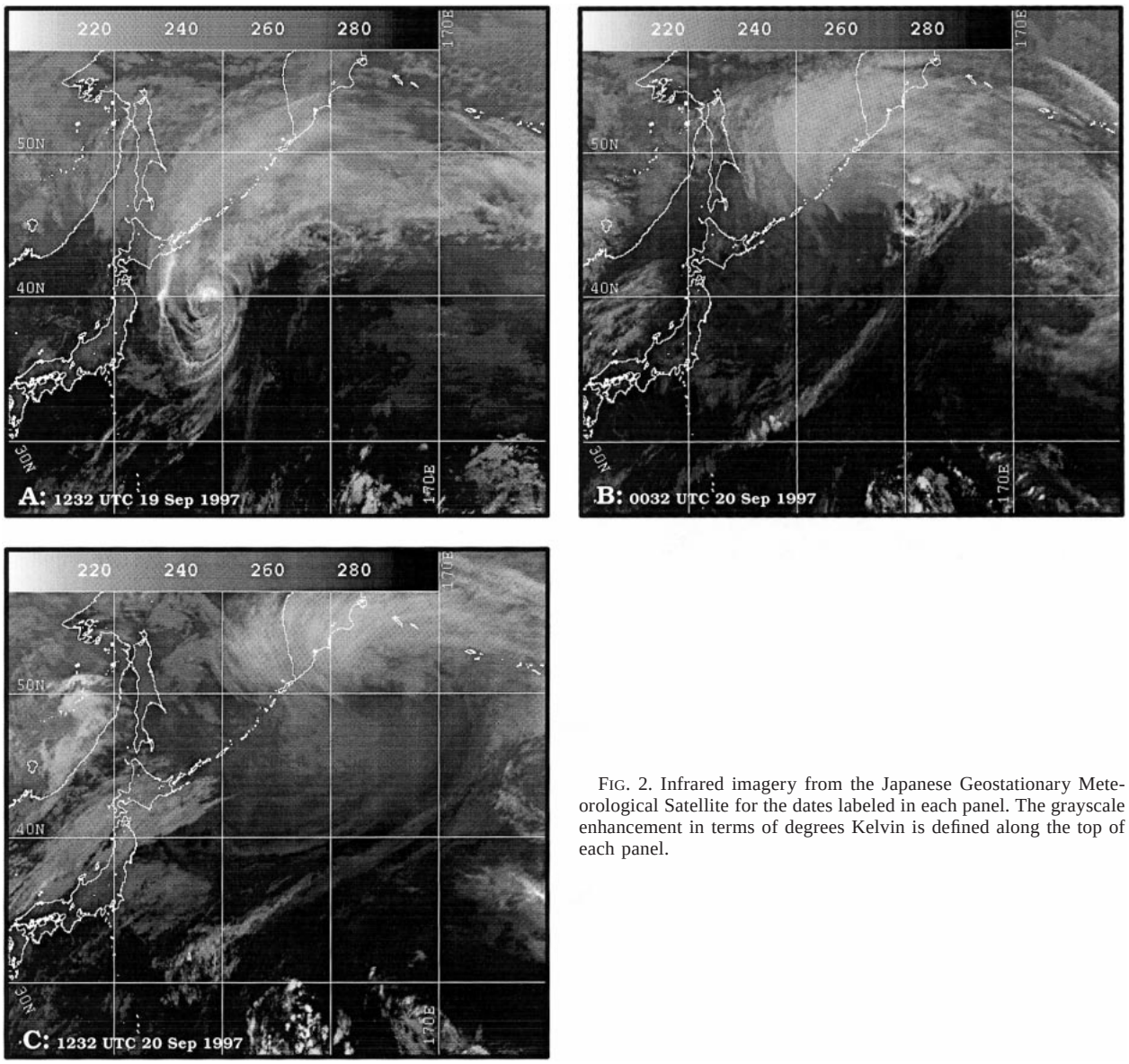

FIG. 2. Infrared imagery from the Japanese Geostationary Meteorological Satellite for the dates labeled in each panel. The grayscale enhancement in terms of degrees Kelvin is defined along the top of each panel.

time, it seems likely that the precipitation pattern was similar to that 12 h prior since the cloud patterns evident in the IR imagery at 1232 UTC 20 September (Fig. 2c) were similar to those 12 h earlier (Fig. 2b).

To examine the three-dimensional flow characteristics during the ET of David, trajectories were computed on isentropic surfaces to implicitly include the adiabatic vertical motion. Because the NOGAPS analyses are not at a fine enough resolution to resolve accurately the trajectories near the TC center, and because diabatic influences would also be large there, trajectories that would only be representative of the broad-scale flow associated with the interaction between David and the midlatitude circulation were examined.

Trajectories were computed by specifying a discrete model formulation to the inviscid equations of motion (Petersen and Uccellini 1979):

$$a_x^{(t)} = -\frac{\Delta\psi}{\Delta x} + f^{(t)}v^{(t)}, \tag{8a}$$

$$a_y^{(t)} = -\frac{\Delta\psi}{\Delta y} - f^{(t)}u^{(t)}. \tag{8b}$$

In this formulation, a_x and a_y are the accelerations in the x and y directions, u is the zonal wind component, v is the meridional wind component, f is the Coriolis parameter, ψ is the Montgomery streamfunction, and the superscript refers to the timestep number. Updated velocity and distance components are calculated by

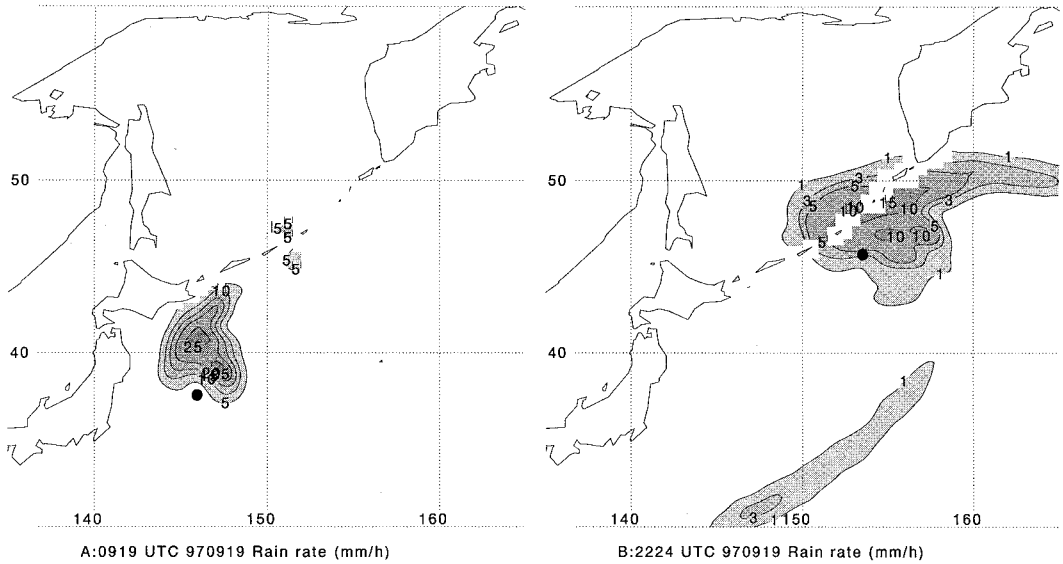

FIG. 3. Rain rates (mm h^{-1}) derived from microwave imagery obtained from polar-orbiting satellites at (a) 0919 UTC 19 Sep and (b) 2224 UTC 19 Sep 1997. The center of the David circulation is marked by the black circle. The contour interval is 5 mm h^{-1} with the 1 and 3 mm h^{-1} contours included in (b).

$$u^{(t+1)} = u^{(t)} + \Delta t\left[\frac{3}{2}a_x^{(t)} - \frac{1}{2}a_x^{(t-1)}\right], \tag{9a}$$

$$v^{(t+1)} = v^{(t)} + \Delta t\left[\frac{3}{2}a_y^{(t)} - \frac{1}{2}a_y^{(t-1)}\right], \tag{9b}$$

$$x^{(t+1)} = x^{(t)} + \frac{1}{2}\Delta t[u^{(t+1)} + u^{(t)}], \tag{9c}$$

$$y^{(t+1)} = y^{(t)} + \frac{1}{2}\Delta t[v^{(t+1)} + v^{(t)}]. \tag{9d}$$

The following starting formulas for the first time step are

$$u^{(1)} = u^{(0)} + a_x^{(0)}\Delta t, \tag{10a}$$

$$v^{(1)} = v^{(0)} + a_y^{(0)}\Delta t. \tag{10b}$$

NOGAPS analyses at 6-h intervals were interpolated using cubic B-splines to the 2-h time step in the trajectory calculations.

Midtropospheric flow patterns were defined by examining three representative trajectories on the 310 K isentropic surface (Figs. 4a,b), which varied between 805 and 410 hPa over the region of interest. Trajectories were purposely chosen away from the immediate environment of the TC. Air parcels that began south and east of David (trajectory path defined by the long-dashed line in Fig. 4) moved northward to the east of David and ascended from 785 to 604 hPa when they turned eastward in the midlatitude flow downstream of the decaying TC. Comparison with satellite imagery (Fig. 2c) suggested that this rising air east of the circulation center became part of the large cloud shield north of the circulation center, which was similar to a warm conveyor belt with forward-sloping ascent as defined by Browning (1990). A second trajectory was chosen to begin at 690 hPa west of the TC near 42°N, 140°E at 0000 UTC 19 September. The air parcels ascended initially to 640 hPa as they passed close to the southern portion of the center. When the decaying TC moved northeastward, the trajectory turned eastward and descended to 767 hPa as part of the westerly flow that moved around the southern portion transforming system. A third representative trajectory began at 423 hPa northwest of David near 47°N, 140°E. Initially, the air parcels moved northeastward as part of the midlatitude wave that was moving off the Asian mainland. When the decaying David also moved northeastward (Fig. 4a), the air parcels were turned toward the southeast and descended to 624 hPa as part of the northwesterly flow to the west of David. The air continued to descend to 793 hPa as it moved around the southern portion of David (Fig. 4b). The trajectories defined a three-dimensional picture of the airflow relative to the transforming system that consisted of rising air that passed east of the center, then turned anticyclonically as part of the large cloud shield north of the center, and descending air that moved southeastward to the west of the center, and then turned toward the east and continued to descend as it passed south of the center.

Klein et al. (2000) define ET as a two-stage process that begins with transformation stage and proceeds to a reintensification stage as an extratropical cyclone. At 1200 UTC 19 September, David was classified as having reached the end of the transformation stage, which was consistent with the satellite image (Fig. 2a) that identified weakening TC characteristics. After 12 h, satellite imagery (Fig. 2b) depicted a large change in the ap-

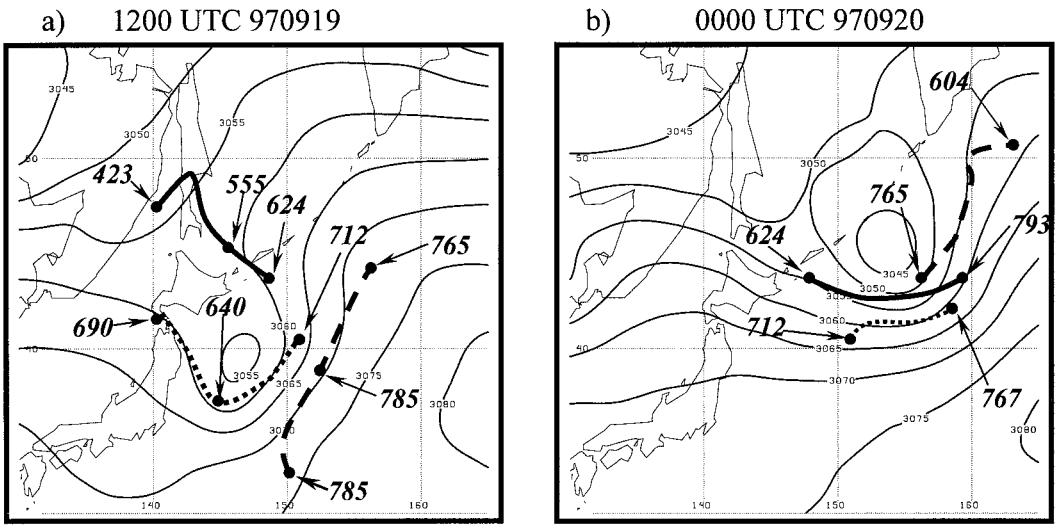

FIG. 4. Montgomery streamfunction (contours in increments of 5 $m^2 s^{-2}$) on the 310 K surface for (a) 1200 UTC 19 Sep 1997 and (b) 0000 UTC 20 Sep 1997, and trajectories for selected parcels. In (a), the first dot on each trajectory is the location at 0000 UTC 19 Sep, the second dot is the location at 1200 UTC 19 Sep, and the third dot is the location at 0000 UTC 20 Sep. The pressure level at each time is indicated by the arrow pointing to the location. In (b), the first dot is the location at 0000 UTC 20 Sep and the second dot is the location at 1200 UTC 20 Sep.

pearance of the transformed system that had entered into the reintensification stage of ET (Klein et al. 2000). Therefore, it was at this time that the structural changes were analyzed with respect to the evolving thermal, vertical motion, and frontal characteristics.

To aid in interpretation of the vector-frontogenesis components at 500 hPa, which was where the maximum amplitudes of the structural changes that impacted the development of frontal characteristics defined by F_n and F_s were found, several synoptic-scale features (Fig. 5) of the evolving ET were examined. The relative vorticity at 500 hPa (Fig. 5a) defined the location of the reintensified cyclone at 45°N, 156°E and the midlatitude trough that was moving off the Asian mainland near 46°N, 146°E. Maximum ascending motion (Fig. 5b) occurred north of the apex of the thermal ridge with descending motion in the thermal trough. A strong dipole thermal advection pattern (Fig. 5c) existed with warm (cold) advection on the east (west) side of the TC center. Complex patterns of divergence and convergence (Fig. 5d) were as expected from the thermal and vorticity advection consideration relative to David and the midlatitude wave.

As defined in (3a), negative F_n defines scalar frontogenesis. Maximum scalar frontogenesis (Fig. 6a) occurred north and east of David with an area of frontolysis west of the center. Although there were small concentrated regions of frontogenesis associated with the convergence/divergence patterns along the thermal wave (Figs. 5d, 6b), the most widespread contribution to F_n was the deformation field (Fig. 6c). To the north and east of the TC center, the axes of dilatation were nearly parallel to the isentropes, which was a deformation pattern consistent with warm frontogenesis when a cyclonic vortex is placed on a baroclinic zone as described by Doswell (1984), Keyser et al. (1988), and Schultz et al. (1998).

A concentrated region of frontolysis along the eastern boundary of the thermal trough near 45°N, 148°E was also dominated by the deformation field (Fig. 6c). Over this region, the axes of dilatation were nearly perpendicular to the isentropes. This structure was similar to frontolytical regions associated with northern portions of cold fronts, which have been identified as ''frontal fractures'' by Shapiro and Keyser (1990). Previous studies of frontal fractures (Neiman and Shapiro 1993; Neiman et al. 1993; Browning et al. 1997) have identified these regions with frontolysis and downward motion of dry air that is typically associated with a tropopause fold (Browning et al. 1997). The trajectory analysis (Fig. 4) indicated that air parcels moving on the 310 K isentropic surfaces descended rapidly over this region.

Over the warm frontogenetic region north and east of the TC center, the gradients of vertical velocity and θ pointed in opposite directions on the poleward side of the baroclinic zone. Therefore, the tilting term in (7a) was frontolytic over this region, which was consistent with the thermally direct circulation implied by the pattern of vertical motion (Fig. 5b) along the trajectory that passed east of the center (Fig. 4b). Similar alignments of the vertical velocity and thermal gradients were found along the eastern boundary of the thermal trough where warm air was rising and moving northward ahead of the cold sinking air associated with the thermal trough.

The structural characteristics defined by the pattern of scalar frontogenesis were also implied by the satellite imagery (Fig. 2b). A large cloud shield existed over the region of warm frontogenesis north and east of the cen-

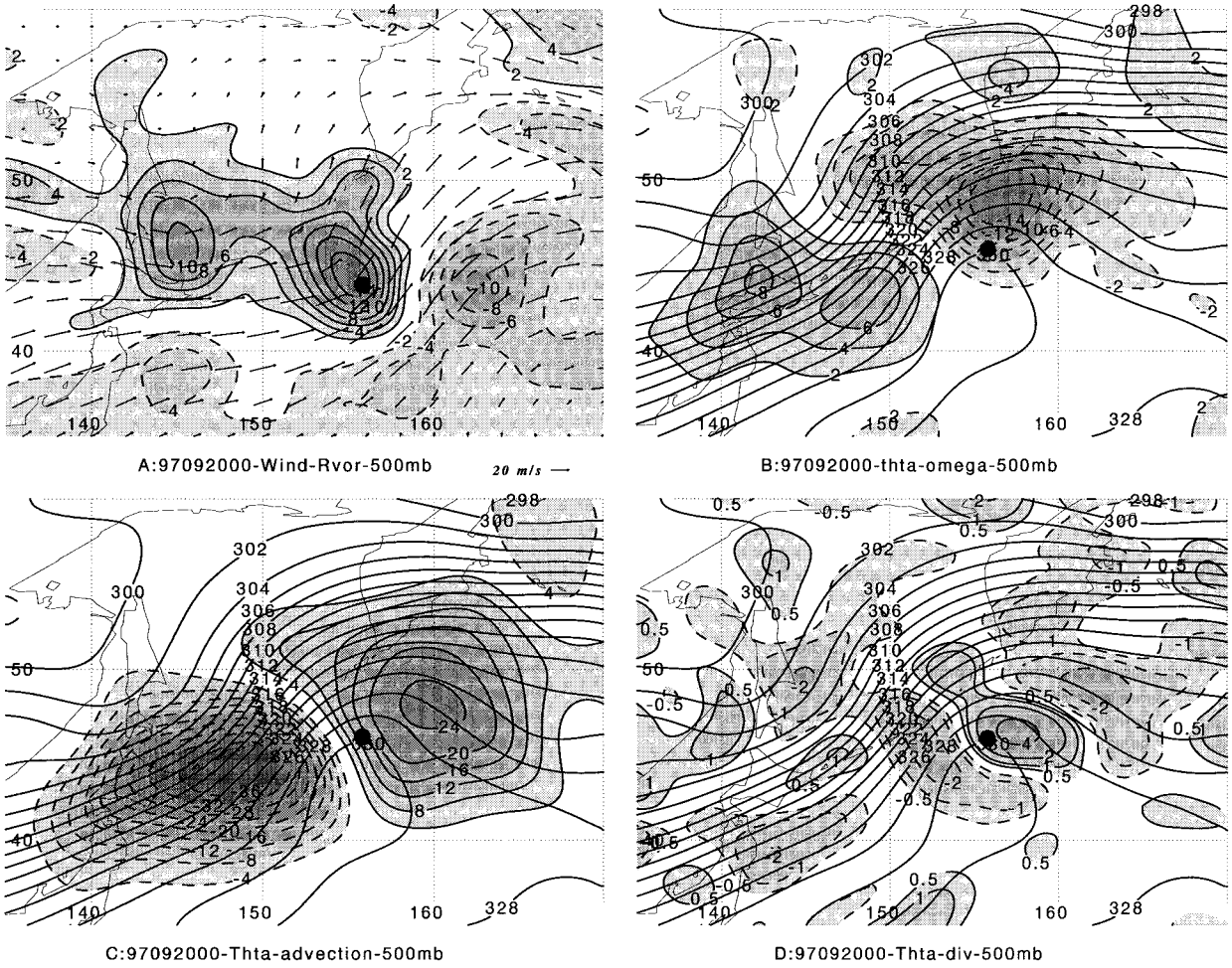

FIG. 5. Values of 500-hPa (a) relative vorticity (contoured and shaded in increments of 2×10^{-5} s^{-1} with negative contours dashed) and wind vectors (see scale in lower right), (b) ω (shaded contours in increments of 2 μb s^{-1} with negative contours dashed) and θ (in 2 K increments), (c) horizontal advection of θ (shaded contours in 4×10^{-5} K s^{-1} increments) and potential temperature as in (b), (d) divergence (shaded contours in increments of 0.5×10^{-5} s^{-1}) and θ as in (b) for 0000 UTC 20 Sep 1997. The black dot marks the location of the low-level center for David.

ter. A large cloud-free area was found west of the center, which was a region of frontolysis. The trajectory analysis, which defined rising (sinking) air north and east (west and south) also corresponded well with the cloud and frontogenesis patterns.

Rotational frontogenesis (Fig. 7a) was dominated by a large region of positive F_s along the eastern boundary of the midlatitude thermal trough, with two regions of weaker negative rotational frontogenesis along the baroclinic zone to the northeast of the center and another weak center to the east near 45°N, 163°E. Whereas the region of positive rotational frontogenesis to the west of the center acted to rotate the $\nabla_h\theta$ in a cyclonic direction, the negative region east of the center acted to rotate the $\nabla_h\theta$ in an anticyclonic direction. Therefore, the rotational frontogenesis component provided dynamical support for amplification of the thermal wave via cold advection to the west and warm advection to the east of the TC center. Examination of the contributions to F_s from the relative vorticity (Fig. 7b) and deformation (Fig. 7c) indicated that deformation dominated along the boundary between the thermal trough and ridge, while relative vorticity dominated near the TC center. The negative contributions to F_s northeast and east of the center were due to the anticyclonic vorticity downstream of the transforming circulation (Fig. 5a). The dipole in vertical motion along the thermal wave pattern (Fig. 5b) with upward motion centered near 48°N, 157°E and downward motion centered near 44°N, 149°E lead to gradients of ω and θ that were perpendicular. Therefore, the tilting frontogenesis term in (7b) would be positive and the contribution to F_s would be negative (Fig. 7d). East of the TC center, the $\nabla_h\omega$ pointed in the opposite direction, which lead to a positive tilting contribution to F_s on the east side of the thermal ridge that was opposite to the contribution due to deformation. The gradient of ω acted to rotate $\nabla_h\theta$ anticyclonically east of the center and cyclonically west

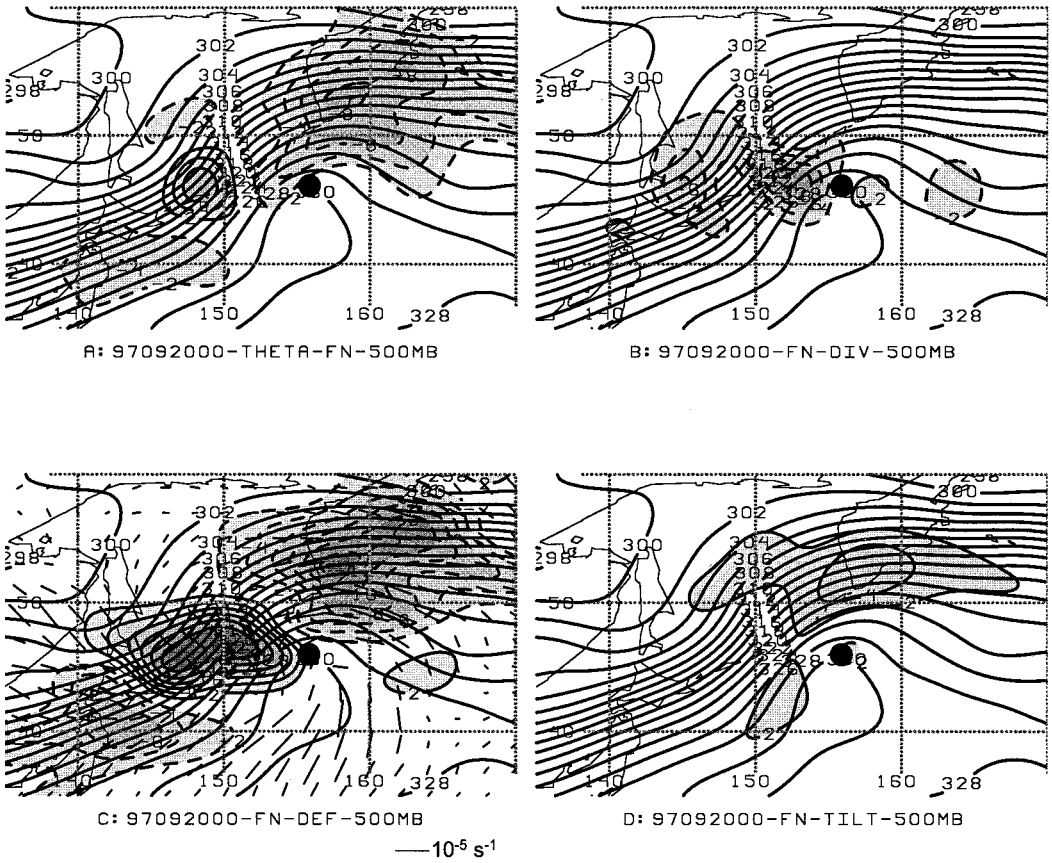

FIG. 6. Potential temperature at 500 hPa (contoured at 2 K intervals) and (a) shaded contours of F_n, (b) shaded contours of F_n-div, (c) shaded contours of F_n-def and axes of dilatation (see scale at lower right), and (d) shaded contours of F_n-tilt. All shaded contours are at intervals of 2×10^{-10} K m^{-1} s^{-1} with negative contours dashed. The black dot marks the location of the low-level center for David.

of the center. Therefore, the contribution due to F_s-tilt acted to flatten the thermal trough, which could be interpreted as a translation of the thermal trough pattern eastward.

Vertical cross sections of total frontogenesis, vertical motion, and relative humidity were used to examine further the structural characteristics associated with the reintensification of the extratropical cyclone that resulted from the ET of David. The vertical cross section (Fig. 8) from the thermal trough to the thermal ridge near a portion of the trajectory depicted by the solid line in Fig. 4 has sinking motion and frontolysis over the region of the thermal trough and its boundary with the thermal ridge. Sinking motion was also implied by the intersection of the 310 K isentrope with the cross section that gives some indication of the path of the air parcel trajectory in Fig. 4 with respect to the cross section. The patterns of sinking motion and frontolysis were representative of regions identified by Neiman and Shapiro (1993) and Neiman et al. (1993) to be associated with frontolysis near the northern portion of boundaries between a thermal trough and ridge in an extratropical cyclone.

The structure of the warm frontogenesis region that existed north and east of the TC center was of importance since the majority of the cloud (Fig. 2b) and precipitation (Fig. 3b) occurred over this region. Vertical cross sections (Fig. 9) oriented north–south along 160°E near the path followed by the trajectory defined by the long dashed line in Fig. 4b are in a region dominated by upward motion and a zone of frontogenesis that sloped from south to north. The slope of the 310 K isentrope on the cross section and the values of vertical velocity indicated that the magnitude of the upward motion through the warm sector of the transforming system was less than the magnitude of the downward motion over the cold sector (Fig. 8), but the integrated effect may have been the same since the parcel path was longer over the warm sector.

Because nearly all of the appreciable precipitation (Fig. 3b) was in the region of warm frontogenesis, it is important to diagnose the contributions to the organization of precipitation over this region. The largest rain rates in bands (Fig. 3b) parallel to the thermal wind suggested a possible mechanism could be slantwise convection due to the release of conditional symmetric in-

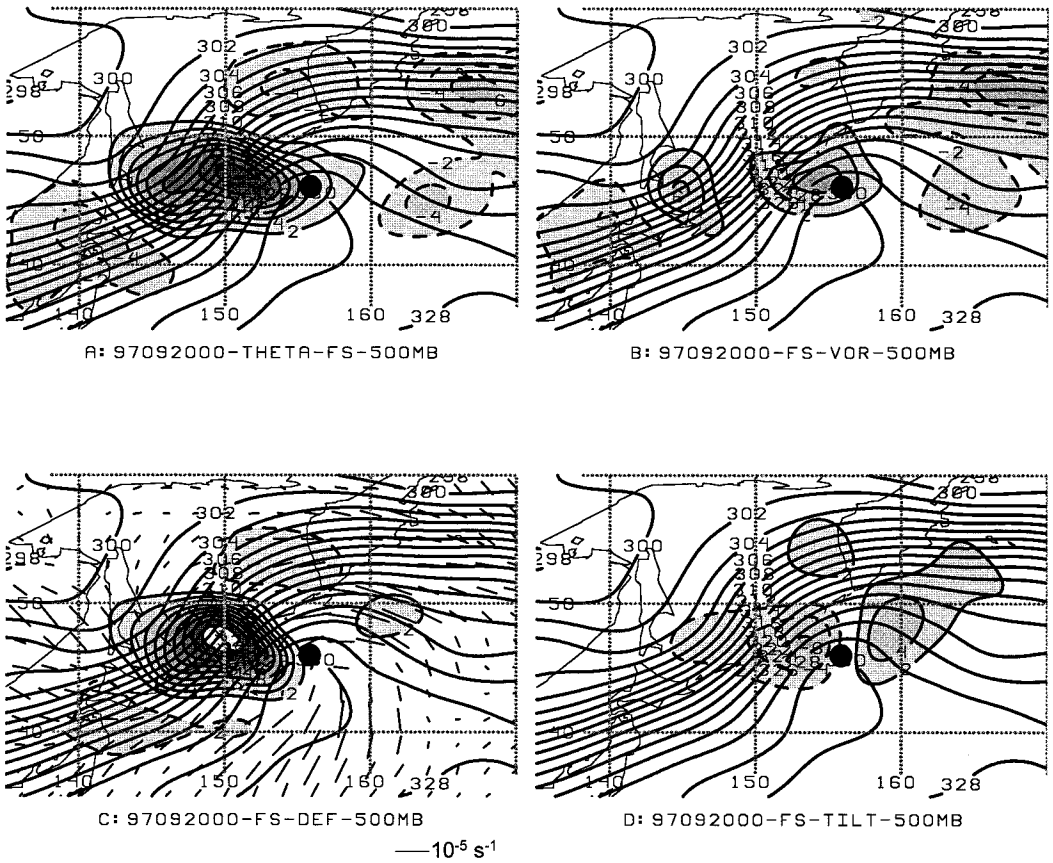

FIG. 7. Potential temperature at 500 hPa (contoured at 2 K intervals) and (a) shaded contours of F_s, (b) shaded contours of F_s-div, (c) shaded contours of F_s-def and axes of dilatation (see scale at lower right), and (d) shaded contours of F_s-tilt. All shaded contours are at intervals of 2×10^{-10} K m^{-1} s^{-1} with negative contours dashed. The black dot marks the location of the low-level center for David.

stability (CSI), in which gravitational and inertial buoyancy determine the displacement of saturated air parcels along a slanted path (Emanuel 1983). This was investigated by assessing whether the necessary ingredients of instability, moisture, and lift necessary for release of CSI (Schultz and Schumacher 1999) existed over the region of warm frontogenesis during the ET of David. Air near the southern portion of the warm frontogenesis and ascent region (Fig. 9a) between 48° and 49°N was also saturated (Fig. 9b). Whereas potential instability requires the vertical gradient of equivalent potential temperature with respect to height be less than 0 (i.e., $\partial\theta_e/\partial z < 0$), conditional instability requires the vertical gradient of saturated equivalent potential temperature with respect to height be less than 0 (i.e., $\partial\theta_e^*/\partial z < 0$). The presence of potential symmetric instability is then defined by the presence of a negative gradient of θ_e along a geostrophic absolute momentum (M_g) surface (i.e., $\partial\theta_e/\partial z|_{M_g} < 0$ with $M_g = v_g + fx$ such that x is taken along a cross section directed from cold air to warm air and v_g is the geostrophic wind). Likewise, CSI is defined by the presence of a negative gradient of θ_e^* along a geostrophic absolute momentum surface (i.e, $\partial\theta_e^*/\partial z|_{M_g} < 0$), so that CSI exists where the isopleths of θ_e^* slope more steeply than isopleths of M_g. Bennetts and Hoskins (1979) and Emanuel (1983) defined this condition to be equivalent to evaluating regions where the saturated equivalent potential vorticity (evaluated as $\text{MPV}_g^* = g\eta_g \cdot \nabla\theta_e^*$ with η_g equal to the geostrophic absolute vorticity) is negative.

A north–south cross section of θ_e (not shown) along 160°E as in Fig. 9 indicated that the region of warm frontogenesis below 900 hPa was a region of potential instability. Browning (1990) indicated that regions of warm conveyor belts are typically regions of potential instability that is released as midlevel convection when the air is lifted over the frontal boundary. A cross section of M_g, θ_e^*, MPV_g^* (Fig. 9c) along 160°E indicated that CSI was also present below 900 hPa at the southern portion of the region of warm frontogenesis. Furthermore, a cross section of M_g, $\partial\theta_e^*/\partial p$, MPV_g^* (Fig. 9d) indicated that this was also a region of conditional instability. Therefore, the region of warm frontogenesis associated with the ET of David was a region where moist gravitational instability (potential instability or conditional instability) and CSI coexisted. In this case,

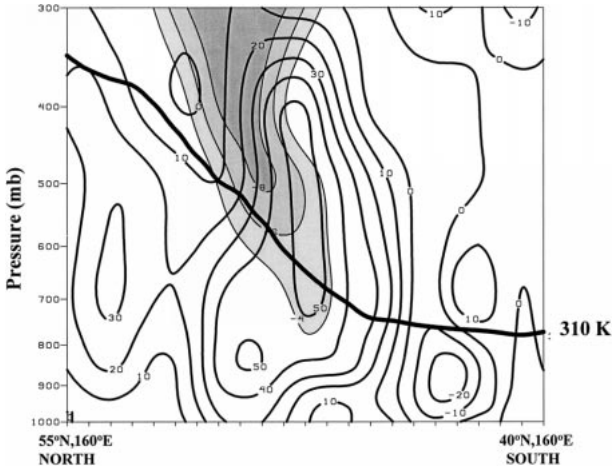

FIG. 8. Vertical cross section of ω (contours in increments of 10 μb s^{-1} and total frontogenesis (shaded contours in increments of 2 $\times$ 10^{-10} K m^{-1} s^{-1} beginning at -4×10^{-10} K m^{-1} s^{-1}) from 55°N, 160°E to 40°N, 160°E. The intersection of the 310 K isentropic surface with the cross section is marked by the thick black line.

it was not possible to state conclusively which process dominated the organization of the precipitation into bands.

Xu (1986) suggested that when both gravitational and symmetric instabilities coexist banded regions of precipitation may form due to ''upscale or downscale development.'' During ET, when the boundary between the warm, moist air east of the decaying TC and the cold, dry midlatitude air north of the TC is well defined, it would appear that the process of downscale development as defined by Xu (1986) would be most responsible for organization of precipitation bands. During downscale development, there is frontal ascent in an environment that contains CSI, which leads to latent heat release and destabilization of the midlevels to gravitational convection. The release of the moist gravitational instability then leads to formation of bands. Since the warm-frontal region was where the active weather appeared to occur during ET, this is an important aspect that may only be addressed adequately through higher space and time resolution fields as could be generated by an accurate simulation with a mesoscale model.

In summary, the development of an extratropical cyclone from the transition of TY David was dominated by the development of a widespread region of warm frontogenesis where nearly all of the cloud cover and precipitation was observed. The deformation field created by the movement of the cyclonic vortex into the midlatitudes was the dominant forcing of warm frontogenesis. No active cold front structure was observed since the cold sector of the thermal wave was dominated by subsidence and frontolysis. The forcing of frontolysis was also dominated by the deformation field. The tilting rotational frontogenesis acted as a mechanism for eastward translation of the thermal pattern. Rotational frontogenesis provided the dynamic support to the patterns of warm (cold) advection to the east (west) of the TC center. Therefore, the patterns of thermal advection due to the vorticity associated with David were reinforced by the midlatitude thermal wave pattern. The primary impact of the rotational frontogenesis was then to contribute to the coupling of the transforming TC with the midlatitude thermal wave, which contributed to the development of an intense extratropical cyclone.

4. Extratropical transition of TY Opal (June 1997)

Although TY Opal (June 1997) moved northward into the midlatitudes ahead of a midlatitude trough, the large-scale midlatitude circulation pattern over the western North Pacific contained a stationary midlatitude cyclone northeast of the decaying Opal (Figs. 10a,b). When Opal moved northeast of Japan at 0000 UTC 21 June (Fig. 10c), the SLP lowered to 987 hPa. Unlike TY David, the ET of TY Opal would be more influenced by the midlatitude primary low pressure system to the northeast than by the broad midlatitude trough to the west. Although a separate low-level pressure center associated with the remnants of Opal was still evident at 1200 UTC 21 June (Fig. 10d), the decaying TC at 500 hPa had already become secondary to the primary midlatitude cyclone located over the Kamchatka peninsula. Beyond 1200 UTC 21 June (not shown), the low-level remnants of Opal also became a secondary circulation that rotated around the primary midlatitude low and eventually moved northward over the Bering Strait.

When Opal moved offshore on 1200 UTC 20 June (Fig. 11a), a band of clouds extended north and east of the TC center to the Asian mainland. Rain rates (Fig. 12) as derived from microwave imagery indicated that a maximum in precipitation existed east of Japan. Geostationary satellite imagery (Fig. 11a) suggested that a separate precipitation maximum might have been located to the north of the center, but the microwave rain-rate algorithm was not applied over land. As Opal moved east of Japan on 0000 UTC 21 June (Fig. 11b), the principal cloud feature continued to extend east–west well north of the low-level center. Microwave imagery (not shown) indicated that this east–west-oriented band was composed of mainly middle and high clouds with some light precipitation. At this time, a link does not seem to exist between Opal and the midlatitude low pressure system to the northeast. After 12 h (Fig. 11c), the high clouds to the north and east of the decaying Opal became thin and appeared to overlie the southern portion of a banded cold frontal feature associated with the midlatitude cyclone. By 0000 UTC 22 June (not shown), the remnants of Opal were merged with the midlatitude cyclone to the northeast.

Air parcels that were south of Opal at 1200 UTC 20 June (Fig. 13a) passed to the east of Opal and ascended when they turned anticyclonically after traveling northeast of Opal (Fig. 13b). This trajectory path was similar to the warm conveyor belt path described in relation to

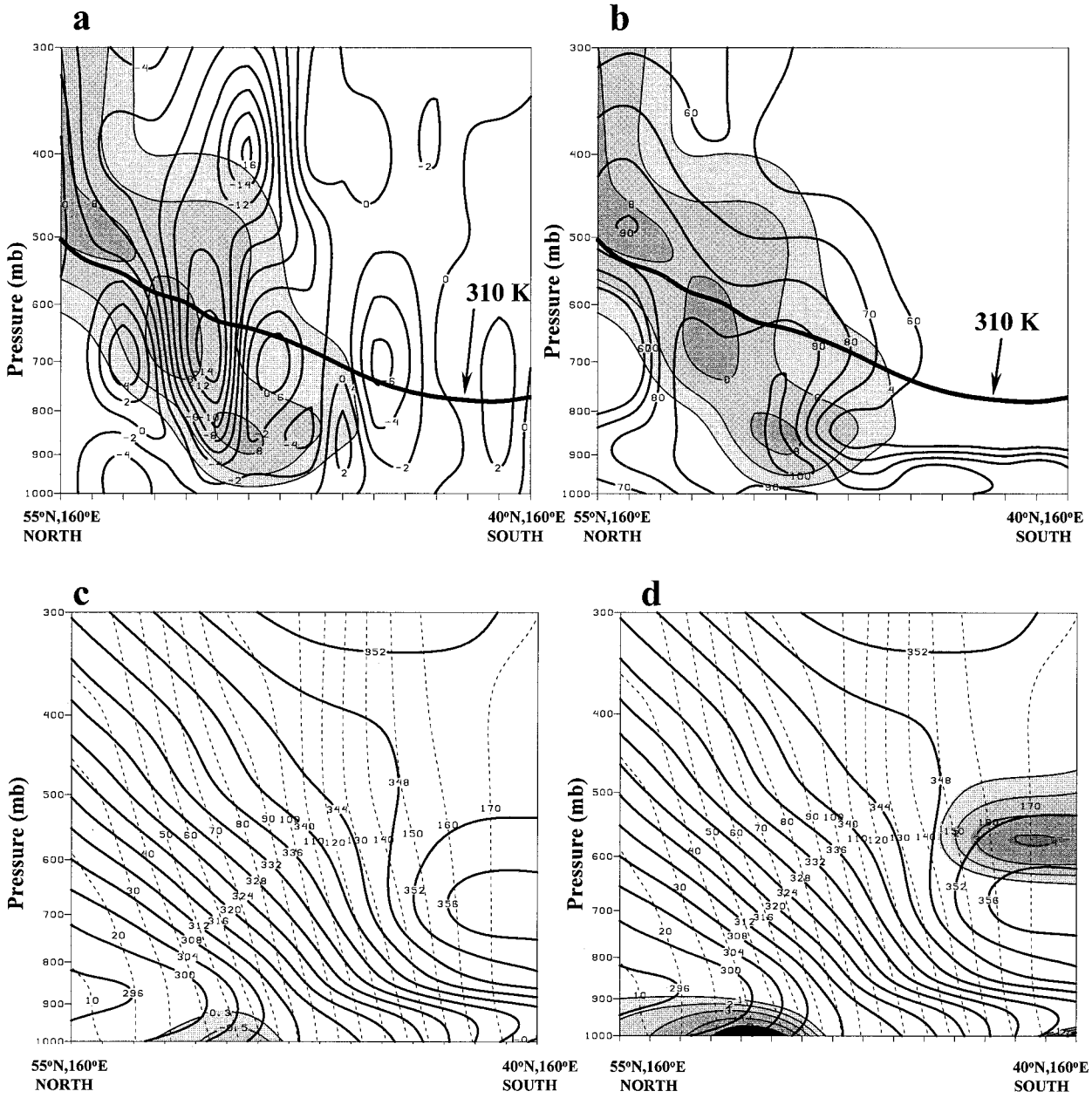

FIG. 9. Vertical cross sections from 55°N, 160°E to 40°N, 160°E of (a) ω (contoured in increments of 2 μb s^{-1}) and total frontogenesis (shaded contours in intervals of 2 $\times$ 10^{-10} K m^{-1} s^{-1} beginning at 4 $\times$ 10^{-10} K m^{-1} s^{-1}); (b) relative humidity (contours in intervals of 10%) and frontogenesis as in (a); (c) θ_e^* (solid contours in increments of 2 K), M_g (dashed contours in increments of 10 m s^{-1}), and MPV$_g^*$ (shaded contours in intervals of 0.2 PVU with 1 PVU equal to 10^{-6} m^2 s^{-1} K kg^{-1}); and (d) θ_e^* (solid contours in increments of 2 K), M_g (dashed contours in increments of 10 m s^{-1}), and shaded contours of $\partial\theta_e^*/\partial p$ in increments of K hPa^{-1}). The intersection of the 310 K isentropic surface with each cross section is marked by the thick black line.

David (Fig. 4). The region of ascent and anticyclonic turning northeast of Opal corresponded to the cloud patterns depicted in Fig. 11c. Air parcels on the western side of Opal (Fig. 13a) were in weak descending flow such that they did not wrap around the decaying TC as did parcels in similar locations with respect to David. Air parcels that began north of Opal did not interact with Opal but traveled around the midlatitude cyclone centered over the Kamchatka peninsula. The air descended when it moved around the southwestern portion of the midlatitude cyclone and north of Opal, which was a cloud-free region in the satellite image (Fig. 11c).

The distribution of the relative vorticity (Fig. 14a) contained a maximum associated with Opal and a second maximum on the cyclonic shear side of the zonal flow between Opal and the midlatitude cyclone north-

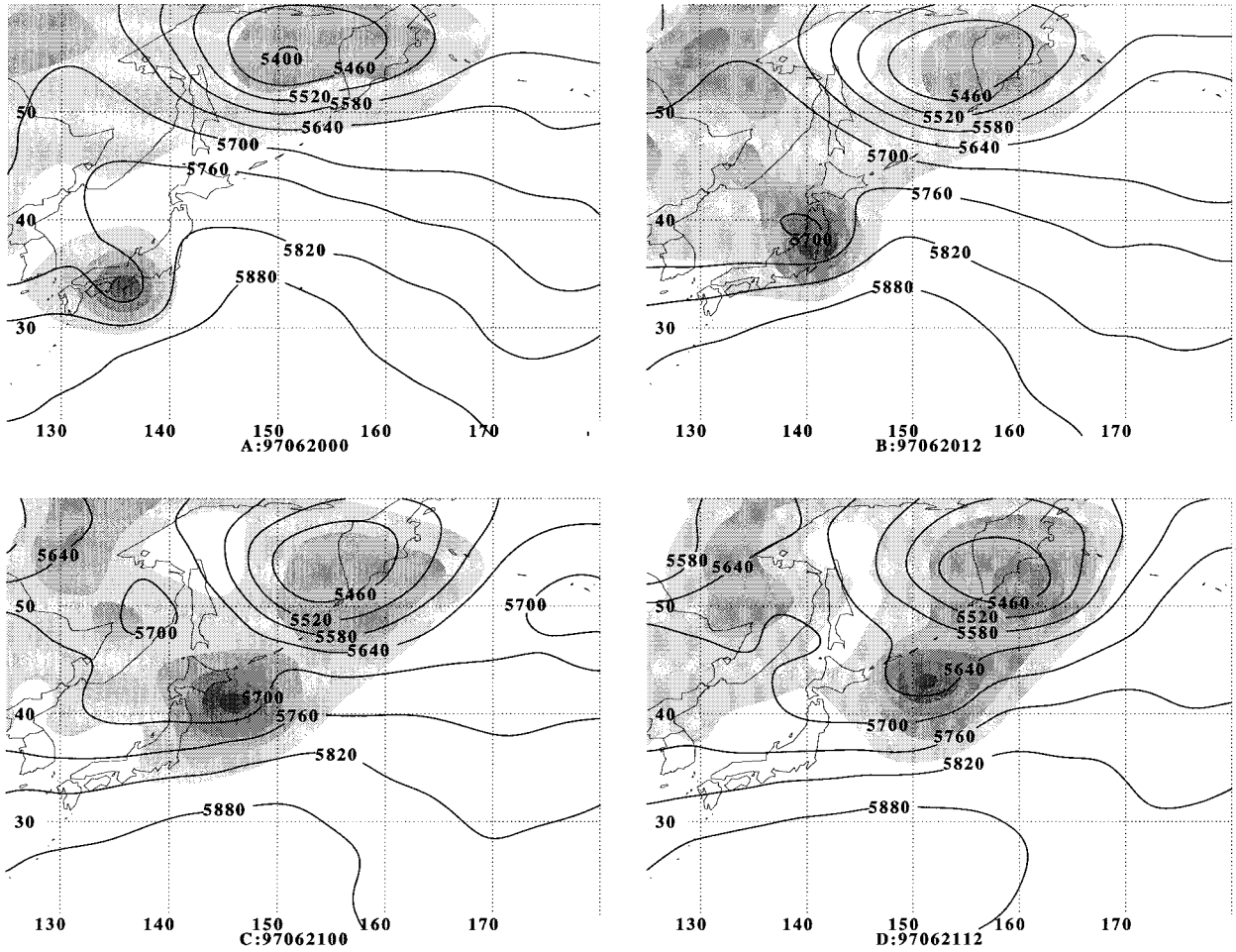

FIG. 10. Analyzed 500-hPa heights (m) and sea level pressure (shaded in 4-hPa increments beginning 1004 hPa) for TY Opal at the times (year, month, day, hour) indicated beneath each panel.

east of Opal. Upward vertical motion extended over a large region northeast of the center of Opal, which was a pattern similar to that associated with the ET of David (Fig. 5b). However, the area of maximum downward motion during the ET of Opal (Fig. 14b) occurred along the flow around the midlatitude cyclone rather than over the thermal trough west of the decaying TC. Only near the center of Opal were the thermal advection patterns (Fig. 14c) similar to patterns associated with David with warm (cold) advection concentrated on the eastern (western) side of the center. There was a dipole of cold and warm advection along the interface between Opal and the midlatitude circulation to the northeast. The divergence pattern (Fig. 14d) was dominated by a zonally oriented convergence region between Opal and the midlatitude cyclone. Whereas patterns of the synoptic-scale fields during the ET of David were dominated by the interaction with the midlatitude trough upstream of David, Opal interacted more with the midlatitude cyclone to the northeast than with the upstream trough.

Scalar frontogenesis (Fig. 15a) was concentrated between Opal and the midlatitude cyclone, which coincided with the location of the primary region of cloud cover that extended north and east of Opal (Fig. 11c). The contribution from the deformation field (Fig. 15c) dominated the pattern of F_n while only a secondary contribution came from the divergence term (Fig. 15b). As in the ET of David, the tilting scalar frontogenesis (Fig. 15d) was frontolytical due to the warm air moving around the eastern side of Opal ascending over the colder air to the north.

The overall pattern of rotational frontogenesis (Fig. 16a) was concentrated in the flow around the midlatitude cyclone north of Opal. Only a secondary center of positive rotational frontogenesis was over the thermal trough to the west of Opal. Although much weaker in this case, the positive rotational frontogenesis in the upstream thermal trough acted to rotate $\nabla_h\theta$ in a cyclonic direction associated with cold advection and deepening of the thermal trough. This positive rotational frontogenesis over the thermal trough west of Opal was due entirely to the deformation field (Fig. 16c) that arose

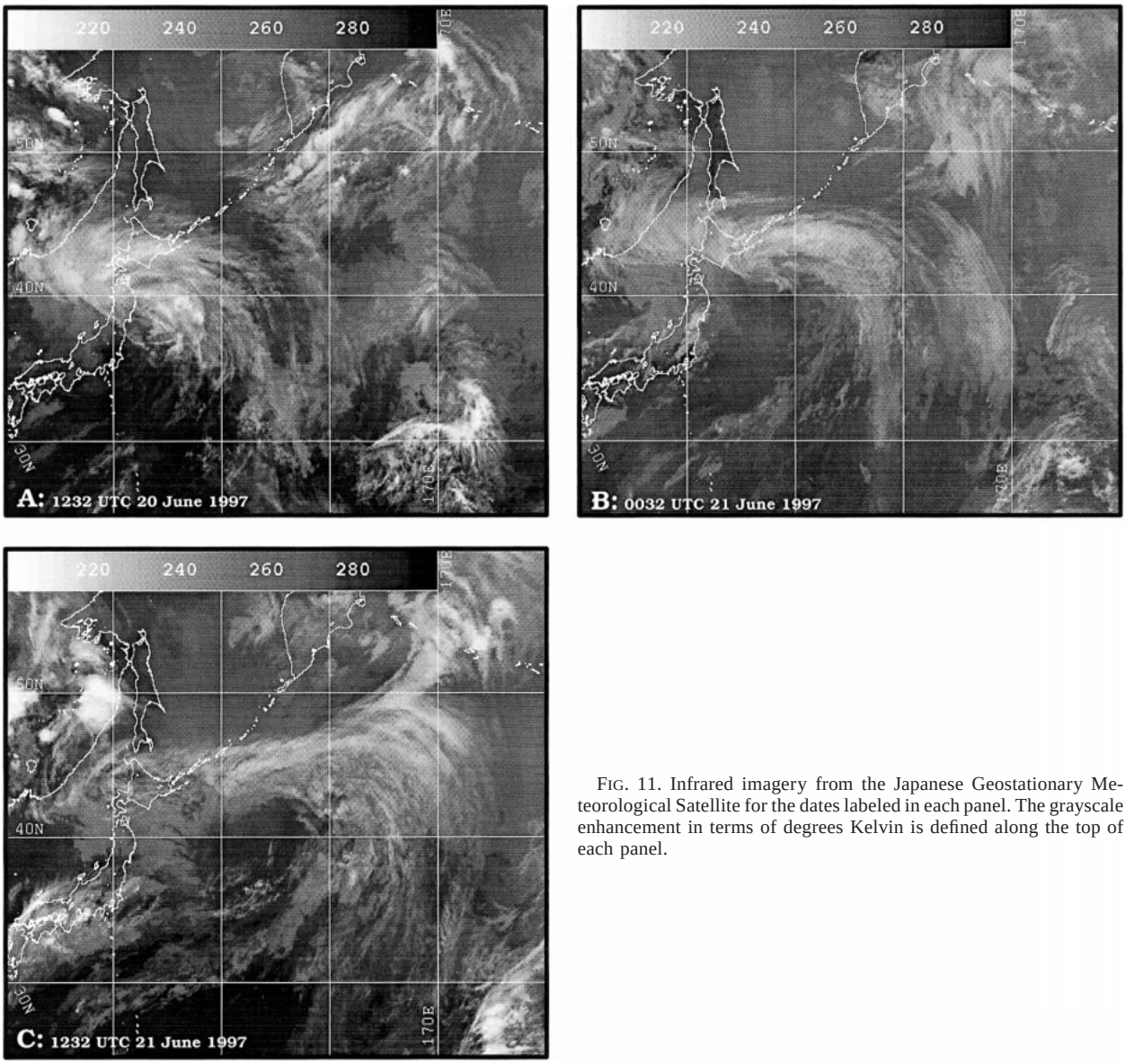

FIG. 11. Infrared imagery from the Japanese Geostationary Meteorological Satellite for the dates labeled in each panel. The grayscale enhancement in terms of degrees Kelvin is defined along the top of each panel.

from the interaction of Opal and the upstream midlatitude system. The large area of positive rotational frontogenesis around the midlatitude cyclone north of Opal was composed of nearly equal contributions from the vorticity (Fig. 16b) and deformation (Fig. 16c) contained in the flow between Opal and the midlatitude cyclone. The concentration of positive rotational frontogenesis between Opal and the midlatitude circulation was supporting dynamically a cyclonic rotation of $\nabla_h \theta$ due to warm advection south of the midlatitude cyclone associated with the poleward movement of Opal and cold advection around the midlatitude cyclone, respectively.

The structure of the warm frontogenetic region during the ET of Opal was very different from that during David (Fig. 9). North-to-south vertical cross sections (Fig. 17) through the region of warm frontogenesis associated with Opal were constructed near the location of the northward movement of the air parcels defined by the trajectory east of Opal in Fig. 13. Below 900 hPa, there was a gradual northward slope to the frontogenetic region (Fig. 17a). Farther north, the region of frontogenesis became nearly vertical as it interacted with the midlatitude cyclone to the north. Upward motion was concentrated on the southern side of the frontogenesis with sinking motion to the north and below the frontogenesis region. Associated with the region of frontogenesis and vertical motion field is a strong gradient of relative humidity with dry air north of the frontogenetic region that was associated with the midlatitude cyclone. The weak warm frontogenetical forcing, vertical motion profile, and strong relative humidity gra-

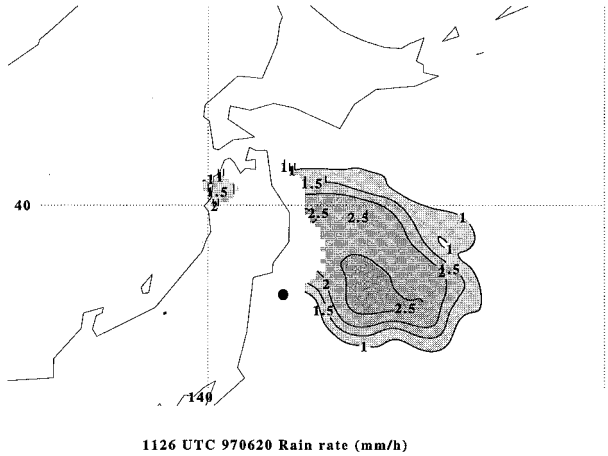

FIG. 12. Rain rates (mm h^{-1}) at 1126 UTC 20 Jun derived from microwave imagery obtained from polar-orbiting satellites. The center of Opal is marked by the black circle.

dient were consistent with satellite imagery (Fig. 11c) that depicted thin clouds over the region with no organized bands of convection.

As in the ET of David, the ET of Opal involved a widespread region of warm scalar frontogenesis that was associated with the deformation field defined by the movement of the cyclonic vortex into the midlatitude flow. However, the pattern of rotational frontogenesis during the ET of Opal was very different from that during the ET of David. Although a small region of rotational frontogenesis occurred over the thermal trough upstream of Opal, the largest amount of rotational frontogenesis occurred due to the deformation flow and vorticity associated with the midlatitude cyclone to the north of Opal.

5. Conclusions and discussion

This study has described different basic characteristics of the cyclones that result from two ET cases of TCs moving into different characteristic midlatitude circulation patterns over the western North Pacific. Each TC moved poleward ahead of a midlatitude trough located west of the TC center. In the case of TY David, the trough was the primary midlatitude circulation feature over the western North Pacific. In the case of TY Opal, the western trough was secondary to a large stationary midlatitude cyclone located to the northeast over the Kamchatka peninsula. The description of the structural changes and complex physical processes as each TC underwent ET was based on the development of frontal regions. Each case was an interaction between a vortex and a baroclinic zone as examined in the context of Doswell (1984) and Keyser et al. (1988). Furthermore, the diagnosis of frontogenesis was partitioned into contributions from scalar frontogenesis and rotational frontogenesis.

The development of frontal characteristics due to scalar frontogenesis was similar for both cases. The deformation field associated with the movement of the TC into the midlatitudes contributed to warm frontogenesis north and east of each TC center. West of each center, the deformation field and sinking motion associated with cold advection contributed to scalar frontolysis. Al-

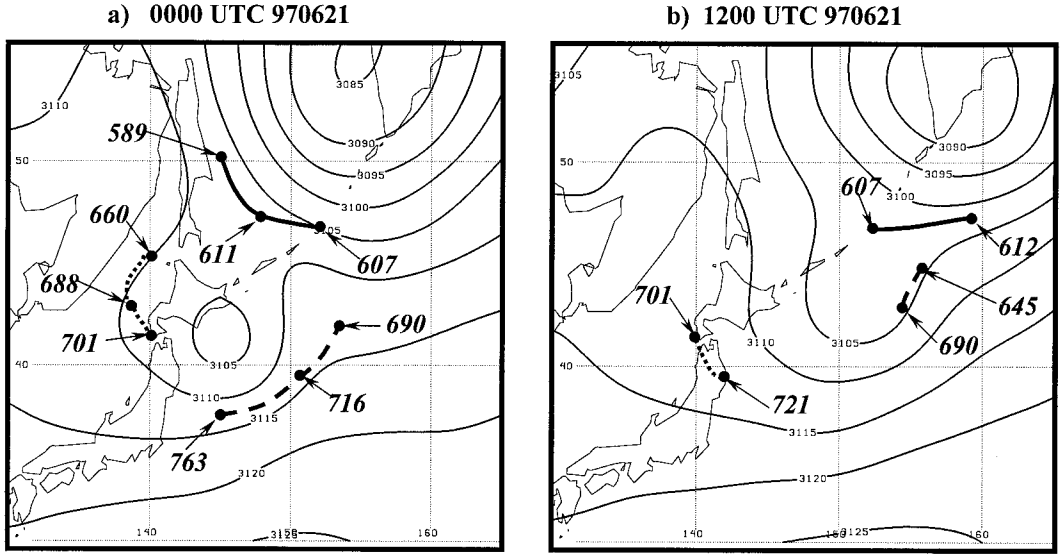

FIG. 13. Montgomery streamfunction (contours in increments of 5 m^2 s^{-2}) on the 310 K surface for (a) 0000 and (b) 1200 UTC 21 Jun 1997 and trajectories for selected parcels. In (a), the first dot on each trajectory is the location at 1200 UTC 20 Jun, the second dot is the location at 0000 UTC 21 Jun, and the third dot is the location at 1200 UTC 21 Jun. The pressure level at each time is indicated by the arrow pointing to the location. In (b), the first dot is the location at 1200 UTC 21 Jun and the second dot is the location at 0000 UTC 22 Jun.

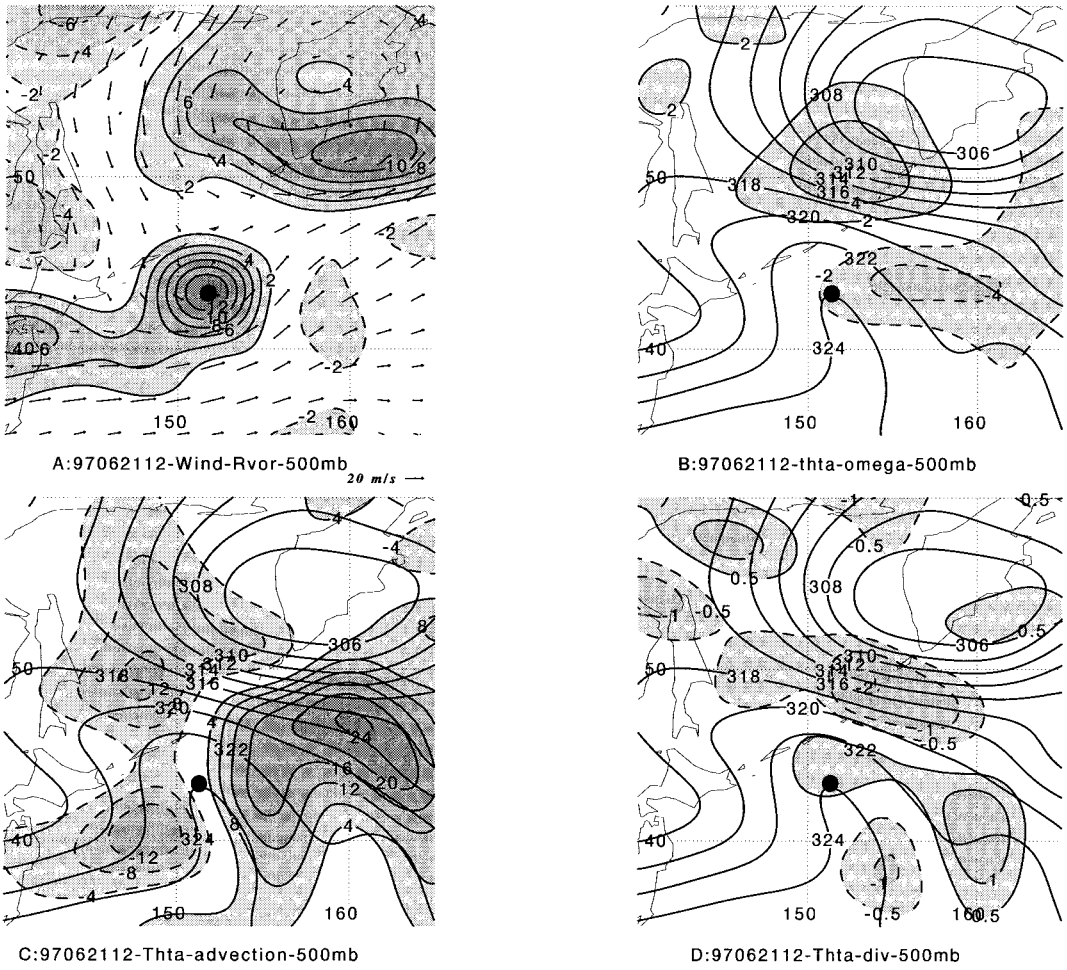

FIG. 14. As in Fig. 5, except for 1200 UTC 21 Jun. The center of Opal is marked by the black circle.

though these general patterns were similar *near* the tropical cyclone, differences in magnitude, areal extent, and structure occurred based on the interactions at the *interface* between each TC and the characteristic midlatitude circulation patterns into which each TC moved. For example, the warm frontogenesis region associated with the ET of Opal was impacted greatly by the presence of the cold midlatitude cyclone to the north. While the strong convergence and deformation between Opal and the midlatitude cyclone contributed to scalar frontogenesis, the frontal zone was prevented from extending northward, which limited large-scale uplift of the warm, moist air that was advected east of Opal. The warm frontal region associated with the ET of David was characterized by an extensive region of slanted vertical motion that contained both gravitational and symmetric instabilities. Therefore, the warm frontal region associated with the ET of David was a region of extensive deep cloud and banded precipitation, while the warm frontal region of Opal contained thin clouds with no appreciable organized precipitation.

The primary difference between the two ET cases was found in the patterns of rotational frontogenesis. For the case of David, rotational frontogenesis provided dynamical support for the warm (cold) advection around the east (west) sides of the TC center. The primary result of the rotational frontogenesis was to amplify the thermal wave by contributing to cyclonic rotation of $\nabla_h\theta$ upstream of David and anticyclonic rotation of $\nabla_h\theta$ downstream of David. This pattern was defined by the deformation field away from the David center and by the relative vorticity nearer to the David center. A smaller tilting rotational frontogenesis contributed to an eastward translation of the thermal wave pattern. The midlatitude circulation pattern into which David moved during ET was such that the dynamical support provided by the rotational frontogenesis and the amplifying thermal wave reinforced each other, which lead to development of a significant extratropical cyclone.

During the ET of Opal, there was weak rotational frontogenesis associated with the thermal wave of with the midlatitude trough. Instead, the primary rotational frontogenesis was concentrated around the midlatitude cyclone north of Opal. The dynamical forcing associated

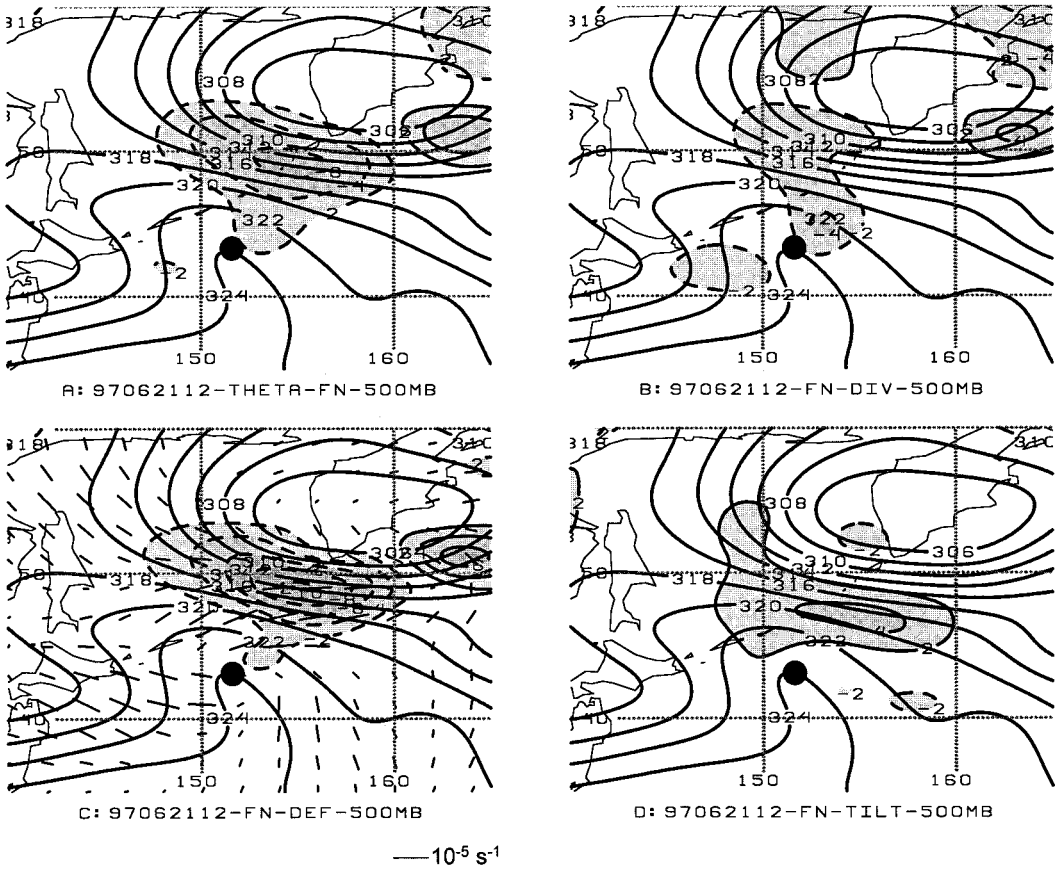

FIG. 15. As in Fig. 6, except for 1200 UTC 21 Jun. The center of Opal is marked by the black circle.

with the thermal advection, vorticity, and deformation upstream of Opal was not large enough to contribute to a significant amplification of the thermal wave into which Opal was moving. Rather, the dynamical support was concentrated north of Opal due to interaction with the stationary midlatitude cyclone. Therefore, the presence of the large stationary midlatitude cyclone prevented Opal from fully coupling with the upstream midlatitude trough and developing into a separate extratropical cyclone. Instead, Opal remained an open wave that moved around the primary cyclone to the north. Although the midlatitude baroclinicity during June when Opal underwent ET was weaker than the September conditions during David, it is felt that the presence of the midlatitude cyclone north of Opal was primarily responsible for the lack of development of a separate extratropical cyclone. For example, TY Peter followed a poleward track similar to Opal and David and underwent ET over the same region approximately eight days after Opal. The difference was the ET of Peter occurred in a circulation pattern similar to that during the ET of David and resulted in a separate intense extratropical cyclone.

One of the unresolved aspects of ET is defining just when transition has occurred. This is important since precipitation and wind patterns evolve rapidly during the transition process and may involve a period of rapid reintensification (Klein et al. 2000). The change from a symmetric TC structure to an asymmetric extratropical cyclone, which in the case of ET includes a warm front that is better defined than a cold front, is proposed as a defining characteristic of the transition progress. That is, the frontogenesis parameter calculated in the region of warm and cold fronts would provide a measure to define the decay of the symmetric TC structure. To examine the utility of this parameter, the evolution of the value of scalar frontogenesis from before transition, through transition, and after transition was examined for each case. A cylindrical grid centered on the TC center is used to compute average frontogenesis at 500 hPa (Fig. 18) over the northeast (i.e., warm-front region) and southwest (i.e., cold-front region) quadrants. In each case, one 12-h period is found in which warm frontogenesis increased rapidly prior to the assigned transition time. During the ET of David (Fig. 18a), warm frontogenesis increased gradually through 1200 UTC 19 September and then a rapid increase occurred over a 12-h period. This timing was also evident in the cloud coverage in the satellite imagery (Figs. 2b,c) The warm frontogenesis associated with Opal (Fig. 18b) does not

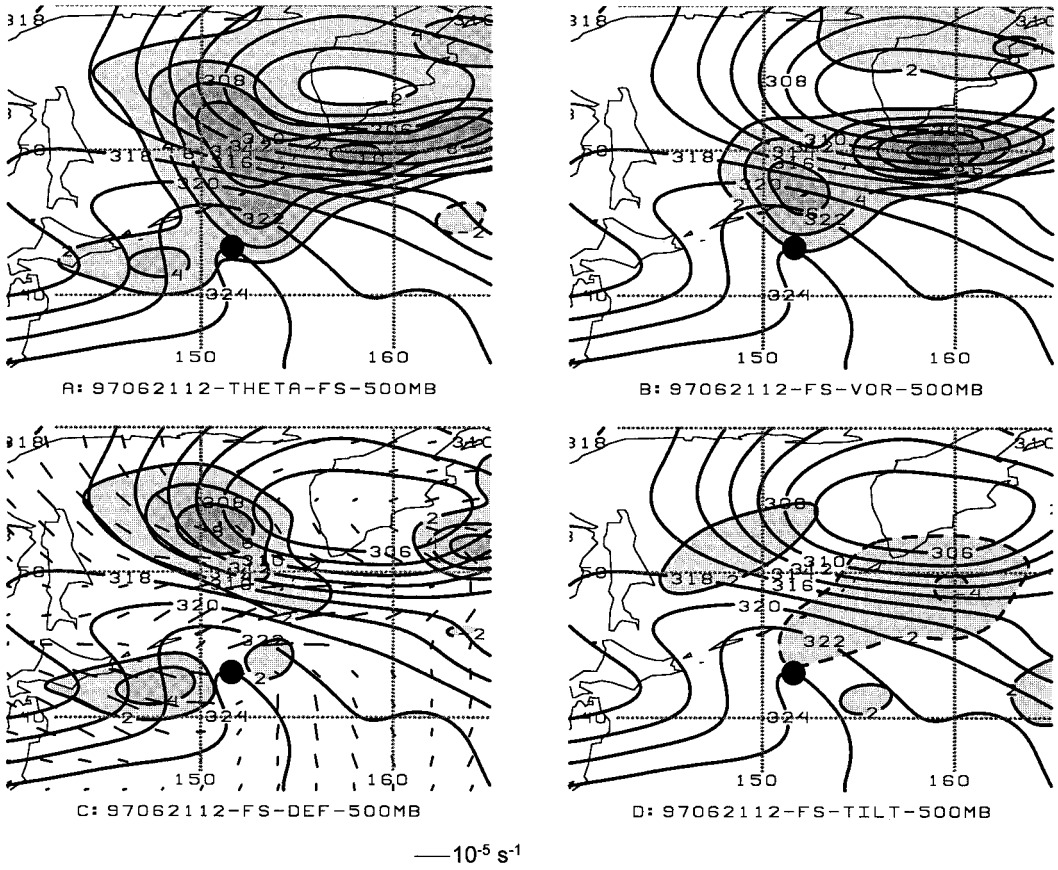

FIG. 16. As in Fig. 7, except for 1200 UTC 21 Jun. The center of Opal is marked by the black circle.

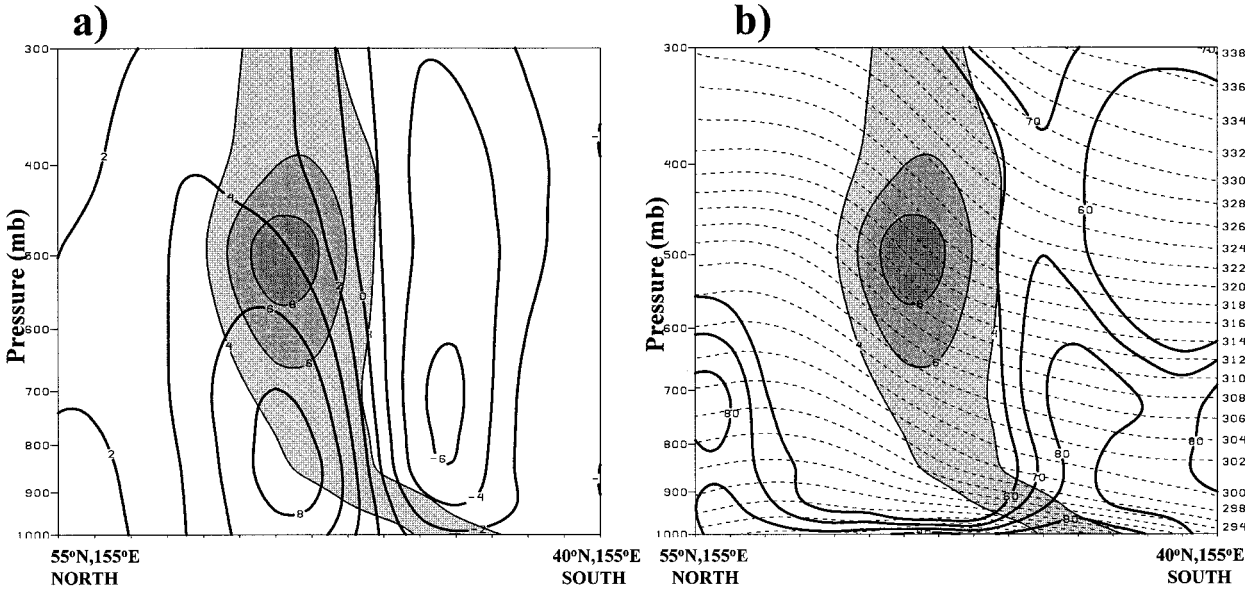

FIG. 17. Vertical cross sections directed from 55°N, 155°E to 40°N, 155°E of (a) ω (contoured in increments of 2 μb s^{-1}) and total frontogenesis (shaded contours in intervals of 2×10^{-10} K m^{-1} s^{-1} beginning at 4×10^{-10} K m^{-1} s^{-1}), and (b) relative humidity (contours in intervals of 10%), frontogenesis as in (a), and θ (dashed contours in increments of 2 K).

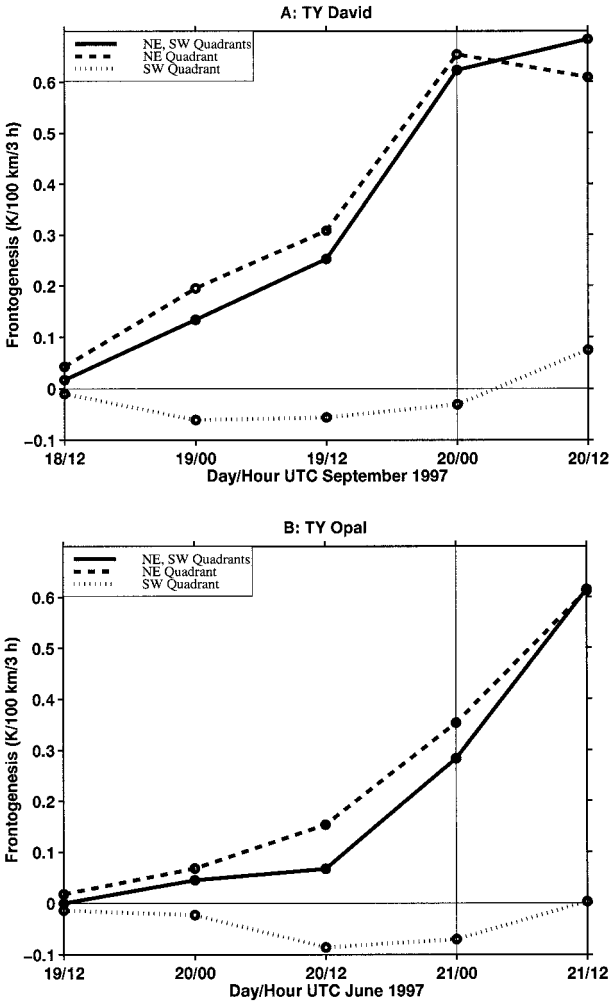

FIG. 18. Average scalar frontogenesis (K 100 km^{-1} 3 h^{-1}) defined over the northeast (NE) and southwest (SW) quadrants of a cylindrical grid centered on each transitioning circulation for the times (day/hour) indicated on the abscissa and for the cases indicated at the top of each panel.

increase appreciably until after 1200 UTC 20 June when Opal begins to approach the midlatitude cyclone to the north. As Opal approached the cyclone, frontogenesis increased rapidly through 1200 UTC 21 June.

Although the ET of David resulted in a large intense extratropical cyclone, the magnitude of scalar warm frontogenesis was not appreciably larger than that associated with Opal. However, the frontal region of David was very active due to presence of instabilities that acted to enhance the response to the frontogenetic forcing. The large warm scalar frontogenesis values associated with Opal were due to the strong convergence and deformation field at the interface between Opal and the midlatitude cyclone. Therefore, frontogenesis values do seem to represent the evolution of the ET process, but they do not provide a measure for the detailed characteristics associated with the weather patterns that might be associated with the ET. For this, a measure of the type of midlatitude circulation pattern into which the TC moves is required.

Although the quadrant averages of frontogenesis as a measure of ET have only been presented for two cases of ET that occurred in different types of midlatitude circulation, a measure of this type could provide useful information on structural characteristics associated with the development of an extratropical cyclone from a TC. A key point to the use of frontogenesis as a measure of ET is the emphasis on synoptic-scale characteristics (i.e., frontal development) rather than changes in the inner core of the decaying TC, which is not easily resolved without high-resolution analyses.

In summary, this study has defined basic characteristics associated with ET of TCs into two characteristic midlatitude circulation patterns over the western North Pacific. In a companion study (Harr et al. 2000), the various structural characteristics are defined in terms of

the fluxes of momentum, potential vorticity, and heat. In this study, the structural characteristics were defined in terms of the forcing of extratropical cyclone features during the transition process. All physical characteristics were related to the large-scale circulation into which the decaying TC was moving. However, variabilities in TC characteristics such as size and intensity plus the role of surface fluxes of heat and moisture need to be addressed in more detail.

Acknowledgments. This research was sponsored by the Office of Naval Research Marine Meteorology Program and the Atmospheric Directorate of the Naval Research Laboratory. The NOGAPS fields were processed at the High Performance Computing Center, Stennis Space Center, Mississippi.

REFERENCES

Anthes, R. A., 1990: Advances in the understanding and prediction of cyclone development with limited-area fine-mesh models. *Extratropical Cyclones, The Erik Palmen Memorial Volume,* C. W. Newton and E. O. Holopainen, Eds., Amer. Meteor. Soc., 221–253.

Bennetts, D. A., and B. J. Hoskins, 1979: Conditional symmetric instability—A possible explanation for frontal rainbands. *Quart. J. Roy. Meteor. Soc.,* **105,** 945–962.

Bosart, L. F., and G. M. Lackmann, 1995: Postlandfall tropical cyclone reintensification in a weakly baroclinic environment: A case study of hurricane David (September 1979). *Mon. Wea. Rev.,* **123,** 3268–3291.

Browning, K. A., 1990: Organization of clouds and precipitation in extratropical cyclones. *Extratropical Cyclones, The Erik Palmen Memorial Volume,* C. W. Newton and E. O. Holopainen, Eds., Amer. Meteor. Soc., 129–153.

——, S. P. Ballard, and C. S. A. Davitt, 1997: High-resolution analysis of frontal fracture. *Mon. Wea. Rev.,* **125,** 1212–1230.

——, G. Vaughan, and P. Panagi, 1998: Analysis of an ex-tropical cyclone after its reintensification as a warm-core extratropical cyclone. *Quart. J. Roy. Meteor. Soc.,* **124,** 2329–2356.

Davies, H. C., C. Schar, and H. Wernli, 1991: The palette of fronts and cyclones within a baroclinic wave development. *J. Atmos. Sci.,* **48,** 1666–1689.

Davies-Jones, R., 1985: Comments on ''A kinematic analysis of frontogenesis associated with a nondivergent vortex.'' *J. Atmos. Sci.,* **42,** 2073–2075.

DiMego, G. J., and L. F. Bosart, 1982a: The transformation of tropical storm Agnes into an extratropical cyclone. Part I: The observed fields and vertical motion computations. *Mon. Wea. Rev.,* **110,** 385–411.

——, and ——, 1982b: The transformation of tropical storm Agnes into an extratropical cyclone. Part II: Moisture, vorticity and kinetic energy budgets. *Mon. Wea. Rev.,* **110,** 412–433.

Doswell, C. A., III, 1984: A kinematic analysis of frontogenesis associated with a nondivergent vortex. *J. Atmos. Sci.,* **41,** 1242–1248.

——, 1985: Reply. *J. Atmos. Sci.,* **42,** 2076–2079.

Emanuel, K. A., 1983: The Lagrangian parcel dynamics of moist symmetric instability. *J. Atmos. Sci.,* **39,** 2152–2158.

Evans, M. S., D. Keyser, L. F. Bosart, and G. M. Lackmann, 1994: A satellite-derived classification scheme for rapid maritime cyclogenesis. *Mon. Wea. Rev.,* **122,** 1381–1416.

Gronas, S., 1995: The seclusion intensification of the New Year's day storm 1992. *Tellus,* **47A,** 733–746.

Harr, P. A., R. L. Elsberry, and T. F. Hogan, 2000: Extratropical transition of tropical cyclones over the western North Pacific. Part II: The impact of midlatitude circulation characteristics. *Mon. Wea. Rev.,* **128,** 2634–2653.

Hogan, T. F., and T. E. Rosmond, 1991: The description of the Navy Operational Global Atmospheric Prediction System's spectral forecast model. *Mon. Wea. Rev.,* **119,** 1786–1815.

Keyser, D., M. J. Reeder, and R. J. Reed, 1988: A generalization of Petterssen's frontogenesis function and its relation to the forcing of vertical motion. *Mon. Wea. Rev.,* **116,** 762–780.

——, B. D. Schmidt, and D. G. Duffy, 1992: Quasigeostrophic vertical motions diagnosed from along- and cross-isentrope components of the Q vector. *Mon. Wea. Rev.,* **120,** 731–741.

Klein, P. M., P. A. Harr, and R. L. Elsberry, 2000: Extratropical transition of western North Pacific tropical cyclones: An overview and conceptual model of the transformation stage. *Wea. Forecasting,* **15,** 373–395.

Liu, G., and J. A. Curry, 1992: Retrieval of precipitation from satellite microwave measurements using both emission and scattering. *J. Geophys. Res.,* **97,** 9959–9974.

Neiman, P. J., and M. A. Shapiro, 1993: The life cyclone of an extratropical marine cyclone. Part I: Frontal-cyclone evolution and thermodynamic air–sea interaction. *Mon. Wea. Rev.,* **121,** 2153–2176.

——, ——, and L. S. Fedor, 1993: The life cycle of an extratropical marine cyclone. Part II: Mesoscale structure and diagnostics. *Mon. Wea. Rev.,* **121,** 2177–2199.

Palmen, E., 1958: Vertical circulation and release of kinetic energy during the development of Hurricane Hazel into an extratropical storm. *Tellus,* **10,** 1–23.

Petersen, R. A., and L. W. Uccellini, 1979: The computation of isentropic trajectories using a ''discrete model'' formulation. *Mon. Wea. Rev.,* **107,** 566–574.

Petterssen, S., 1956: *Weather Analysis and Forecasting.* Vol. 1, *Motion and Motion Systems,* 2d ed., McGraw-Hill, 428 pp.

Schultz, D. M., and C. A. Doswell III, 1999: Conceptual models of upper-level frontogenesis in southwesterly and northwesterly flow. *Quart. J. Roy. Meteor. Soc.,* **125,** 2535–2562.

——, and P. N. Schumacher, 1999: The use and misuse of conditional symmetric instability. *Mon. Wea. Rev.,* **127,** 2709–2732.

——, D. Keyser, and L. F. Bosart, 1998: The effect of large-scale flow on low-level frontal structure and evolution in midlatitude cyclones. *Mon. Wea. Rev.,* **126,** 1767–1791.

Shapiro, M. A., and D. Keyser, 1990: Fronts, jet streams and the tropopause. *Extratropical Cyclones, The Erik Palmen Memorial Volume,* C. W. Newton and E. O. Holopainen, Eds., Amer. Meteor. Soc., 167–191.

Shimazu, Y., 1998: Classification of precipitation systems in mature and early weakening stages of typhoons around Japan. *J. Meteor. Soc. Japan,* **76,** 437–445.

Sinclair, M. R., 1993: Synoptic-scale diagnosis of the extratropical transition of a southwest Pacific tropical cyclone. *Mon. Wea. Rev.,* **121,** 941–960.

——, and M. J. Revell, 2000: Classification and composite diagnosis of extratropical cyclogenesis events in the southwest Pacific. *Mon. Wea. Rev.,* **128,** 1089–1105.

Thorncroft, C. D., B. J. Hoskins, and M. E. McIntyre, 1993: Two paradigms of baroclinic-wave life-cycle behavior. *Quart. J. Roy. Meteor. Soc.,* **119,** 17–55.

Velden, C. S., C. M. Hayden, S. J. Nieman, W. P. Menzel, S. Wanzong, and J. S. Goerss, 1997: Upper-tropospheric winds derived from geostationary satellite water vapor observations. *Bull. Amer. Meteor. Soc.,* **78,** 173–195.

Xu, Q., 1986; Conditional symmetric instability and mesoscale rainbands. *Quart. J. Roy. Meteor. Soc.,* **112,** 315–334.